UNIVERSITY OF CALIFORNIA

Los Angeles

Transverse Liquid Fuel Jet Breakup, Burning, and Ignition

A thesis submitted in partial satisfaction of the

requirements for the degree Master of Science

in Mechanical Engineering

by

Hsi-shang Li

1990

The thesis of Hsi-shang Li is approved.

Owen I. Smith

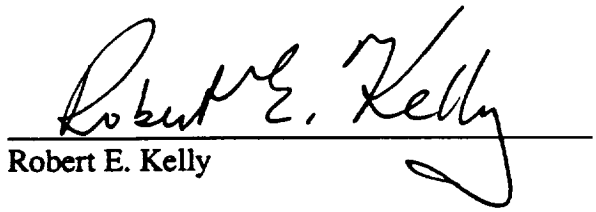

Robert E. Kelly

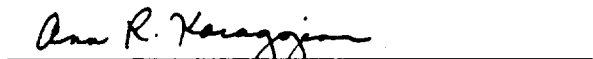

Ann R. Karagozian, Committee Chair

University of California, Los Angeles

1990

TABLE OF CONTENTS

LIST OF FIGURES

NOMENCLATURE

Roman Letters

Ar	frequency coefficient of Arrhenius equation
B_o	transfer number
C	molar density
C_p	specific heat at constant pressure
D	coefficient of mass diffusion
E_a	activation energy
h	step size of discretization
h_i	enthalpy of species i
h_i^o	energy of formation of species i
h_o	half-spacing of vortices
J	jet-to-crossflow momentum flux ratio $\equiv \frac{\rho_j U_j^2}{\rho_\infty U_\infty^2}$
M	effective Mach number
M_∞	free stream Mach number
M_F	molar weight of fuel
M_O	molar weight of oxidizer
p	pressure
Q	heat of reaction per unit mass of fuel
Q_l	laten heat of vaporization
R	blunt body position
Re	Reynolds number

Ru	universal gas constant
s,y	coordinates along jet trajectory
T	temperature
U_j	jet velocity at orifice
U_o	local velocity of liquid free stream
U_∞	free stream velocity
u_{ij}	velocity of each grid point
W	twice the semi-minor axis of the ellipse
X,Z	coordinates associated with jet trajectory
x,y	coordinates along jet cross-section surface
Y_O	mass fraction of oxidizer
Y_F	mass fraction of fuel

Greek letters

α	oxidizer-fuel stoichiometric ratio
β	pressure gradient parameter
Γ_s	effective circulation of surface flow about jet cross-section
δ	boundary layer thickness
θ	angle denoting position about jet cross-section
λ	thermal conductivity
μ	dynamic viscosity
ν	kinematic viscosity
ρ	density

σ	surface tension coefficient
ϕ	angle indicating orientation of jet trajectory
ψ	compressible stream function
ξ,η	coordinates associated with Levy-Lee's transformation
ξ_b,η_b	coordinates associated with blunt body grid generation
r,θ_b	coordinates associated with blunt body
ω	mass consumption rate

Subscipt

e	external flow
F	fuel
g	gas
i	species i
ij	grid point
j	jet condition
l	liquid
o	oxidizer
w	wall condition
∞	free stream condition

ACKNOWLEDGMENTS

First of all I would like to thank my thesis advisor, Prof. A. R. Karagozian, for her direction, encouragement and support in this work.

I am also indebted to Dr. Trinh T. Nguyen for extensive discussions on the liquid jet model and the use of the computer code. Thanks are also sincerely extended to Prof. J. M. McDonough, Prof. O. I. Smith, and Prof. R. E. Kelly for their constructive comments regarding the scope of this study.

Finally, I would like to express my sincere gratitude to my parents, Mr. and Ms. Chen-Hwan Li, for their love and guidance.

This work has been supported by NASA Ames/Dryden Research Center under Grant NCC 2-374, by the U.S. Department of Energy under Grant DE-FG03-88ER13910, and by the Engineering System Analysis for the Control of Toxics (ESACT) Program at UCLA.

ABSTRACT OF THE THESIS

Transverse Liquid Fuel Jet Breakup, Burning, and Ignition

by

Hsi-shang Li

Master of Science in Mechanical Engineering

University of California, Los Angeles, 1990

Professor Ann R. Karagozian, Chair

An analytical/numerical study of the breakup, burning, and ignition of liquid fuels injected transversely into a hot air stream is conducted. The non-reacting liquid jet breakup location is determined by the local sonic point criterion first proposed by Schetz, et al. (1980). Two models, one employing analysis of an elliptical jet cross-section and the other employing a two-dimensional blunt body to represent the transverse jet, have been used for sonic point calculations. An auxiliary criterion based on surface tension stability is used as a separate means of determining the breakup location. For the reacting liquid jet problem, a diffusion flame supported by a one-step chemical reaction within the gaseous boundary layer is solved along the ellipse surface in subsonic crossflow. Typical flame structures and concentration profiles have been calculated for various locations along the jet cross-section as a function of upstream Mach numbers. The integrated reaction rate along the jet

cross-section is used to predict ignition position,which is found to be situated near the stagnation point. While a multi-step reaction is needed to represent the ignition process more accurately, the present calculation does yield reasonable predictions concerning ignition along a curved surface.

CHAPTER I

INTRODUCTION

In the past there has been a great deal of interest in the mechanisms of breakup, decomposition, atomization, and burning associated with the transverse liquid fuel jet. This reacting flowfield is typically present in air-breathing combustors, in which the crossflow of air can be subsonic (e.g., in the turbojet) or supersonic (as in the scramjet). Liquid transverse jets are also frequently used as a means of introducing liquid hazardous waste into an incinerator, where the crossflow can be considered to be nearly incompressible. It is the purpose of the present modeling effort to explore the physical mechanisms of jet breakup that can be crucial in the prediction of fundamental jet behavior, as well as some of the mechanisms related to fuel jet ignition and burning.

In terms of transverse liquid jet breakup, surface wave mechanisms, stripping-type breakup, and liquid surface stability are several popular and successful approaches which can be used to predict fundamental behavior of the liquid. Generally, the global breakup process can be divided along the jet into four parts-- the curved column zone, the fractured clump zone, the spray zone, and the atomization zone (see Less and Schetz (1986)). Figure 1 is a schematic description of this representation for supersonic crossflow. Initially, in the curved column zone, the liquid forms a circular, coherent column of fluid. As the liquid penetrates the high-

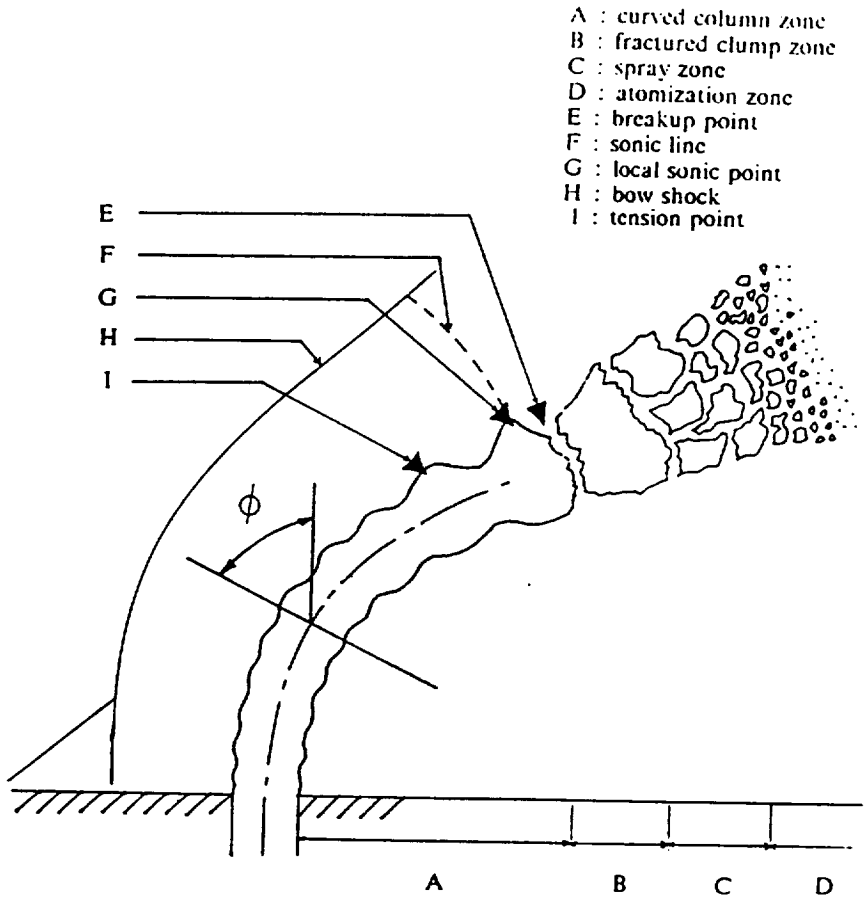

Figure 1 Schematic of transverse liquid jet breakup processes.

speed crossflow, axial waves develop and propagate with increasing amplitude and speed along the surface of the jet column. At the same time, the jet curves downstream due to aerodynamic forces and typically fractures at the trough of a high-amplitude wave. In the early stages of this zone, surface tension holds the liquid column together, although eventually, it works with the aerodynamic forces to fracture the column and decompose the liquid fragment. In this transient stage, from the clump zone to the spray zone, the surface tension instability mechanism plays a leading role in the breakup process. Finally, in the atomization zone, the droplets mix with the turbulent air stream and are vaporized. Although the breakup mechanisms have been studied in some detail by experimental researchers (e.g., Clark (1964), Sherman (1971), and Schetz, et al. (1980)), there is still no overall criterion for this complicated phenomenon that can exactly predict the location of jet breakup.

One emphasis of the present study with respect to liquid breakup is to be able to predict the beginning point of breakup in supersonic streams using a non-empirical model incorporating compressibility effects, one of which has been shown previously to predict liquid jet behavior well (Heister, et al. (1989), Nguyen (1989)). Schetz, et al. (1980) first observed that the local sonic point associated with a sharp wave crest is a rather good indicator for the beginning of breakup. The liquid jet column fractures shortly behind the local sonic point, where the jet body has turned some 25-30 degrees from the initial vertical. It is this observation which will be explored in one aspect of the present study. Two different analytical/numerical models are used for comparison here to study the influence of the local sonic point on breakup. First, the model used by Nguyen (1989) (see also Heister, et al. (1989)), in which numerical solution of the gas flow about locally two-dimensional slices of the liquid jet

is used to predict jet behavior, is incorporated to estimate the local sonic point on the surface of the liquid jet. The second approach assumes the trajectory of the liquid jet to be an effectively two-dimensional blunt body, with numerical solution of the air stream around the liquid jet, from which a local sonic point also may be estimated.

An examination of the effects of surface tension and aerodynamic forces on jet breakup has also been undertaken by a number of researchers. Clark's (1964) experimental study of the influence of internal and external forces in the breakup process reveals that, though the surface tension at the liquid interface tends initially to restore the liquid to its original cross-sectional shape, in the later stages of the breakup process, it actually assists the aerodynamic forces (external forces) in the process of disintegration. The studies by Sherman and Schetz (1971) and Nejad and Schetz (1972) explore the balance between the effects of viscosity and surface tension for transverse liquid jet breakup. We employ their ideas in reasoning that when the internal (surface tension) and external (aerodynamic) forces are of the same order, their global contribution to the breakup process will begin to be significant. Another aspect of the present analysis thus determines the position at which these forces are of the same order, again as a means of estimating breakup location.

In consideration of the self-ignition of a fuel jet injected transversely into a hot stream, the following major questions arise: 1) what is the primary mechanism that triggers this spontaneous chemical process and causes flame spreading, and 2) where does this phenomenon first happen? An examination of the fundamental physical mechanisms and chemical kinetics associated with the laminar diffusion flame surrounding the liquid jet is thus necessary to explore ignition. Many theoretical in-

vestigations into combustion at a liquid surface have been confined to the cases in which the chemical reaction, whether it occurs in the gas phase or at the surface, is considered to take place at an infinitely fast rate (e.g., Crespo and Linan (1975), and Burke (1928)). The model for the transverse liquid fuel jet in subsonic crossflow has thus far considered only fast chemistry (Nguyen (1989)). A study by Chung (1965), however, which examines the chemically reacting nonequilibrium boundary layer problem, reveals that the most interesting features of the problem are due to the coupling of the boundary layer characteristics and the finite-rate chemical reaction, and are completely lost in the equilibrium limit (fast chemistry). It is only in cases where the chemical reaction takes place with a finite rate that the true behavior of a chemically reacting boundary layer, including ignition processes, becomes manifest. It is thus of interest to examine the effects of finite rate chemistry on the liquid transverse jet problem.

By incorporating finite rate chemistry into the present problem, we are able to study the ignition phenomena associated with the jet's gaseous boundary layer. A considerable problem in the study of ignition mechanisms is the question of an ignition criterion. In most experiments, the measurements of ignition-delay time are based on the detection of light emission (e.g., Baev, et al. (1984), and Kashiwagi and Summerfield (1972)). The concept of the integrated reaction rate through the boundary layer as a method for estimating ignition, first introduced by Kashiwagi and Summerfield (1972), has been shown to yeild reasonable predictions, particularly for burning particles. It is this concept that is used here as an ignition criterion. Although no specific experimental data are available in the present problem for direct comparison, the results from this model should be fairly useful in studying the con-

trolling properties of the diffusion flame and predicting trends related to ignition.

CHAPTER II

OVERVIEW OF THE TRANSVERSE LIQUID FUEL JET MODEL

Owing to the complicated nature of turbulent mixing in the liquid jet in compressible flow, early modeling efforts focused on empirical descriptions of the jet trajectory and pressure distribution (see Catton, et al. (1968) and Adelberg (1967)). More recently, experimental studies have evaluated shock dynamics, droplet size, wave phenomena, and interface stability of the jet (e.g., Less and Schetz (1986), Schetz, et al. (1980), and Nejad and Schetz (1972)). Among the important observations made by these researchers is the complex shock structure which forms in association with the transverse jet (see Figure 1). Whether laminar or turbulent, the gaseous boundary layer on the flate plate upstream of the jet separates, and forms a shock which attaches itself to the dominant bow shock partially surrounding the jet. While lateral jet spread is seen to be strongly dependent on upstream Mach number, the actual degree of jet penetration depends more strongly on the jet-to-crossflow momentum flux ratio and pressure ratio (Kolpin, et al. (1969)). The cross-section of the liquid jet is determined to deform into a characteristic "horseshoe" or "kidney" shape as a result of the pressure and shear fields present in the flowfield (Forde, et al. (1966)). This type of deformed cross-section is also observed to occur in jets injected transversely into crossflow of the same phase (see Kamotani and Greber (1972), Fearn and Weston (1974), and Karagozian (1986a)), as a result of the formation of a vortex pair structure associated with the jet cross-section. This type of vortical struc-

ture also dominates the behavior of the gaseous fuel jet (diffusion flame) in crossflow (see Brzustowski (1976), Broadwell and Breidenthal (1984), and Karagozian (1986b)).

The recent experimental efforts by Less and Schetz (1986) indicate the importance of the jet-to-crossflow dynamic pressure ratio in predicting the structure and behavior of the liquid jet, and the desirability to operate future liquid injection systems at high dynamic pressure ratios, making use of the superior atomizing characteristics of certain liquid fuels. These researchers also note the correlation between liquid jet breakup (in both subsonic and supersonic crossflow) and the Strouhal number associated with vortices shed past a circular or elliptical surface. This observation implies a relationship between transverse liquid jet breakup and the generation of vorticity at the liquid-gas interface, which results in the formation of vortical structures within the liquid jet and the characteristic kidney-shaped cross-section.

The present vortex model is described in detail in Heister, Nguyen, and Karagozian (1989) for the non-reacting liquid jet in supersonic crossflow, and in Nguyen and Karagozian (1989) for the reacting jet in subsonic crossflow. In these studies, the jet trajectory, flame characteristics (if present), and the external flow structure are predicted and compared with experimental data. The primary assumption employed is that the jet behavior may be determined by examining the dynamics of locally two-dimensional slices of the liquid jet, taken perpendicular to its centerline. Slices of the liquid jet are represented by the elliptical cross-section of a vortex pair recirculation cell, consistent with experimental observations (e.g., Forde, et al. (1966), Kamotani and Greber (1972), and Fearn and Weston (1974)). For supersonic

crossflow, a locally two-dimensional shock wave dominates the airflow around the jet cross-section. The external flow approaches the ellipse at an effective Mach number $M=M_\infty \sin(\phi)$, where M_∞ is the upstream Mach number and ϕ is the inclination angle of the jet slice taken with respect to the vertical. The bow shock enveloping the jet causes the gas to become locally subsonic in the stagnation region of the jet cross-section, although the flow can become supersonic as it accelerates about the elliptical surface. Consistent with the representation of inviscid two-dimensional flow about the elliptical jet cross-section (external to the gas boundary layer), the conservation of mass, momentum, and energy are governed by the conservative two-dimensional Euler equations. The computer code for solving this system of equations of gas dynamics is constructed in finite volume form for arbitrary two-dimensional skewed grid cells and is based on the first-order, time-dependent numerical scheme developed by Godunov, Zabrodin, and Prokopov (1961). A grid generation scheme using elliptical coordinates is developed.

Two useful computational results from this model are provided in Figures 2 and 3. Figure 2 describes the bow shock position about an ellipse for different upstream Mach numbers. All external flow properties (pressure, density, etc.) can be calculated using this scheme. Figure 3 details the variation in velocity components along the surface of the ellipse. The inviscid flow about the surface is used to "drive" the solution of the external gas boundary layer. As a result of the external aerodynamic forces, a gas boundary layer develops along the elliptical liquid surface and a much thinner liquid boundary layer forms simultaneously inside the liquid-gas interface. The present situation is complicated by the fact that the velocity of the liquid at the interface is non-zero, since the external (gaseous) flow drives the internal

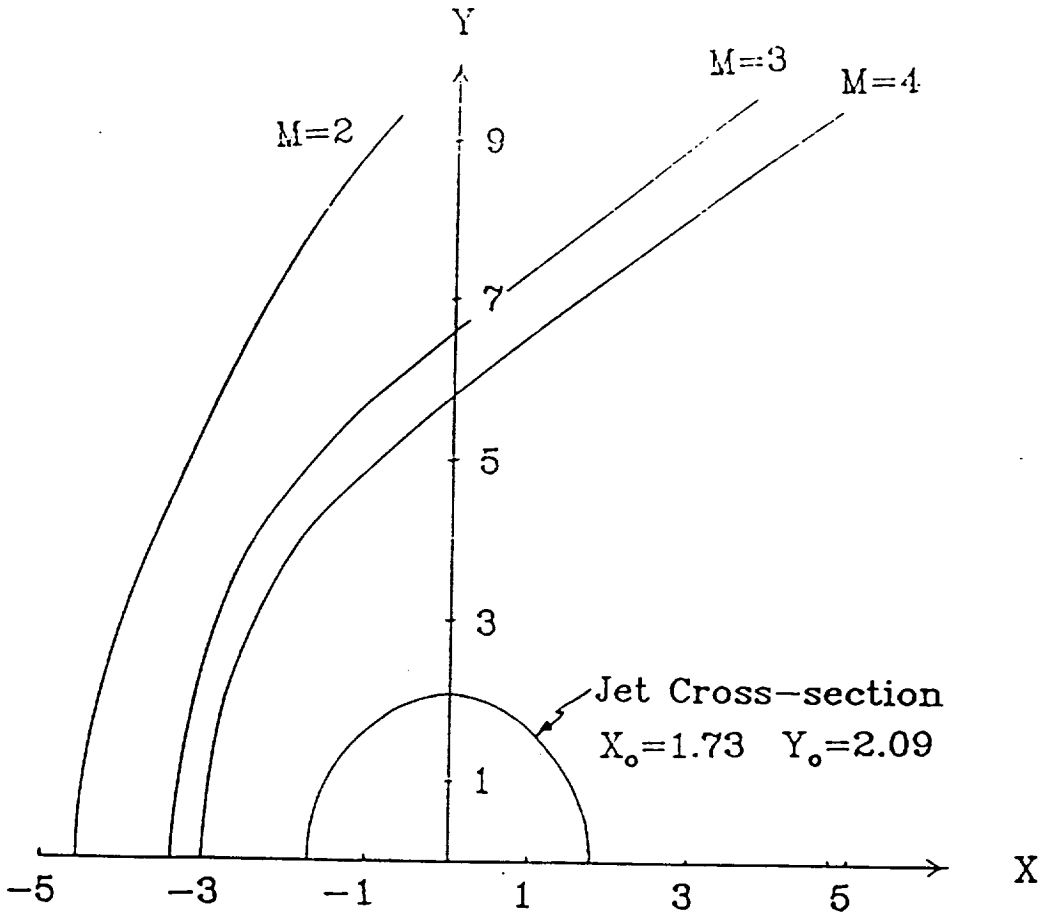

Figure 2 Computed shapes of bow shocks formed ahead of elliptical cross-section (from Heister, et al.(1989)).

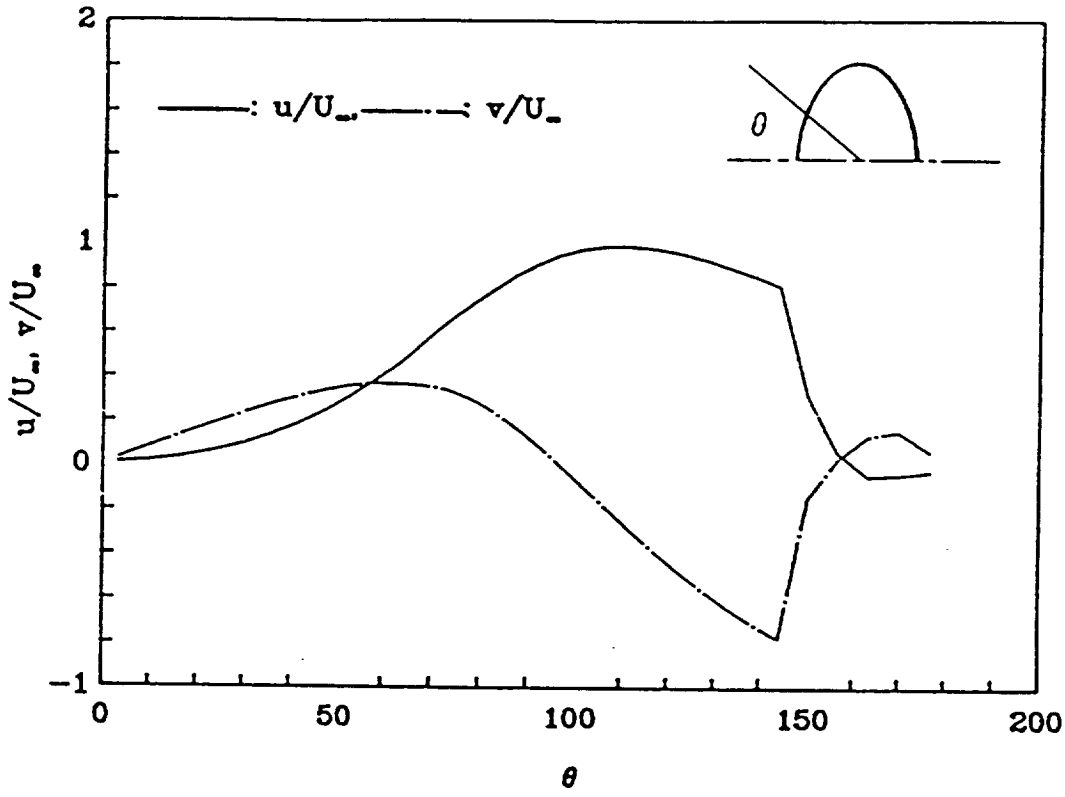

Figure 3 Computed velocity components along ellipse surface for effective Mach number M=2 (from Heister, et al.(1989)).

(liquid) flow within the jet cross-section. In order to examine the dynamic interaction between the liquid jet and the external gas flow, an incompressible vortex pair is used to represent the internal liquid flow field, again consistent with experimental observations (see Forde, et al. (1966), Kamonati and Greber (1972), and Fearn and Weston (1974)). Coupling to liquid and gaseous boundary layers reasonably reproduces the dynamics of the two-phase flow problem.

The main purposes of this liquid jet modeling effort (see Heister, et al. (1989) and Nguyen and Karagozian (1990)) are to explore the nature of vorticity generation in the problem of transverse liquid jet, to evaluate its effect on the local drag associated with the jet cross-section and, ultimately, its effect on jet penetration and trajectory. The drag acting on the elliptical cross-section of the jet is calculated by incorporating the inviscid flow solution about the ellipse as the "outer flowfield" seen by the external (gaseous) boundary layer of the jet cross-section. Calculation of the growth of the external boundary layer, and determination of the local shear stress acting along the liquid-gas interface, is performed using the approximate techniques of Gruschwitz (1950) and Flugge-Lotz and Johnson (1955) for compressible boundary layers. The Gruschwitz solution, which employs a fourth order polynomial to approximate flow in a gaseous boundary layer, is used from the stagnation point to the shoulder (top) of the ellipse, while the Flugge-Lotz and Johnson solution (employing a fifth order polynomial) is used from the shoulder to the point of separation. The dual methods are employed here because of the superior ability of the fifth order polynomial solution to predict separation. Details of the computational procedures for calculating velocity profile, displacement and momentum thickness as well as pressure distribution and shear stress corresponding to the ellipse surface are described by

Heister et al. (1989).

An effective drag coefficient C_D associated with the jet cross-section is now determined by the integration of the shear stress as well as the pressure distribution along the liquid-gas interface. It is assumed that, beyond the separation point, the pressure acting at the surface is averaged between the computed pressures at the separation and rearward stagnation point, a method shown to be reasonable by Gonor (1980). Hence, for different upstream conditions (e.g., Mach number) seen by the local jet cross-section, an approximate drag coefficient for the elliptical cross-section may be computed according to the above procedure. Figure 4 shows this computed result as a function of the effective Mach number, with comparison made to empirical data for flow over a cylinder (a result used in earlier transverse jet models (Catton, et al. (1968) and Adelberg (1967))). Based on this determination of the drag coefficient C_D, the force balance perpendicular to the jet trajectory may be performed.

The turning of the liquid jet is then determined by coupling the results of the force balance to mass and momentum balances along the jet trajectory. The mass loss due to droplet shedding is taken into account at each cross-section of the jet through stripping of the internal viscous layer (after Gonor (1980)). Typical results for the predicted jet trajectories (and bow shock if present) are shown in Figures 5ab. These results indicate that the present analytical/numerical model accurately represents both the external gas flow and the internal liquid flow so that appropriate jet behavior is predicted. Moreover, this model makes possible the determination of characteristic properties important to breakup mechanisms.

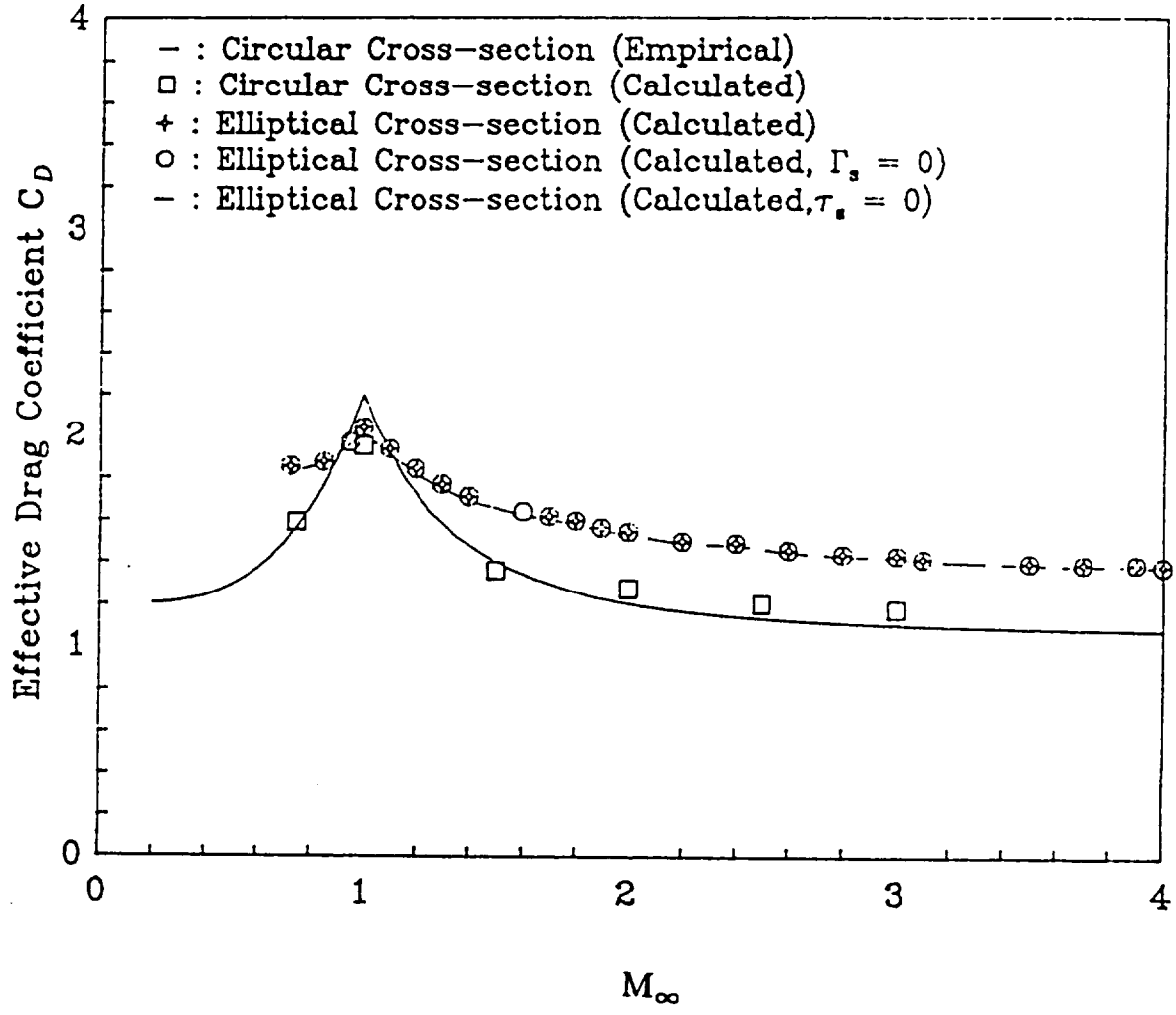

Figure 4 Computed drag coefficient C_D distribution with upstream Mach number (from Heister, et al.(1989)).

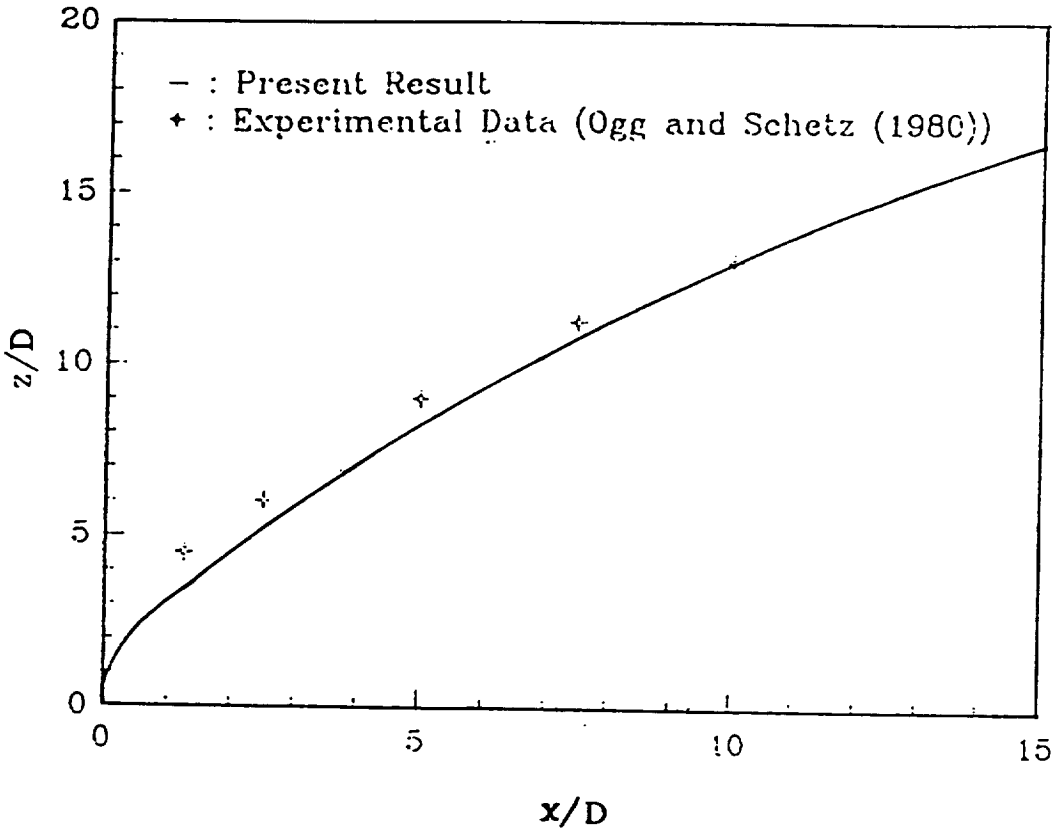

Figure 5a Computed jet trajectory for $M_\infty = 0.6, J = 5$, compared with experimental results (from Nguyen and Karagozian (1990)).

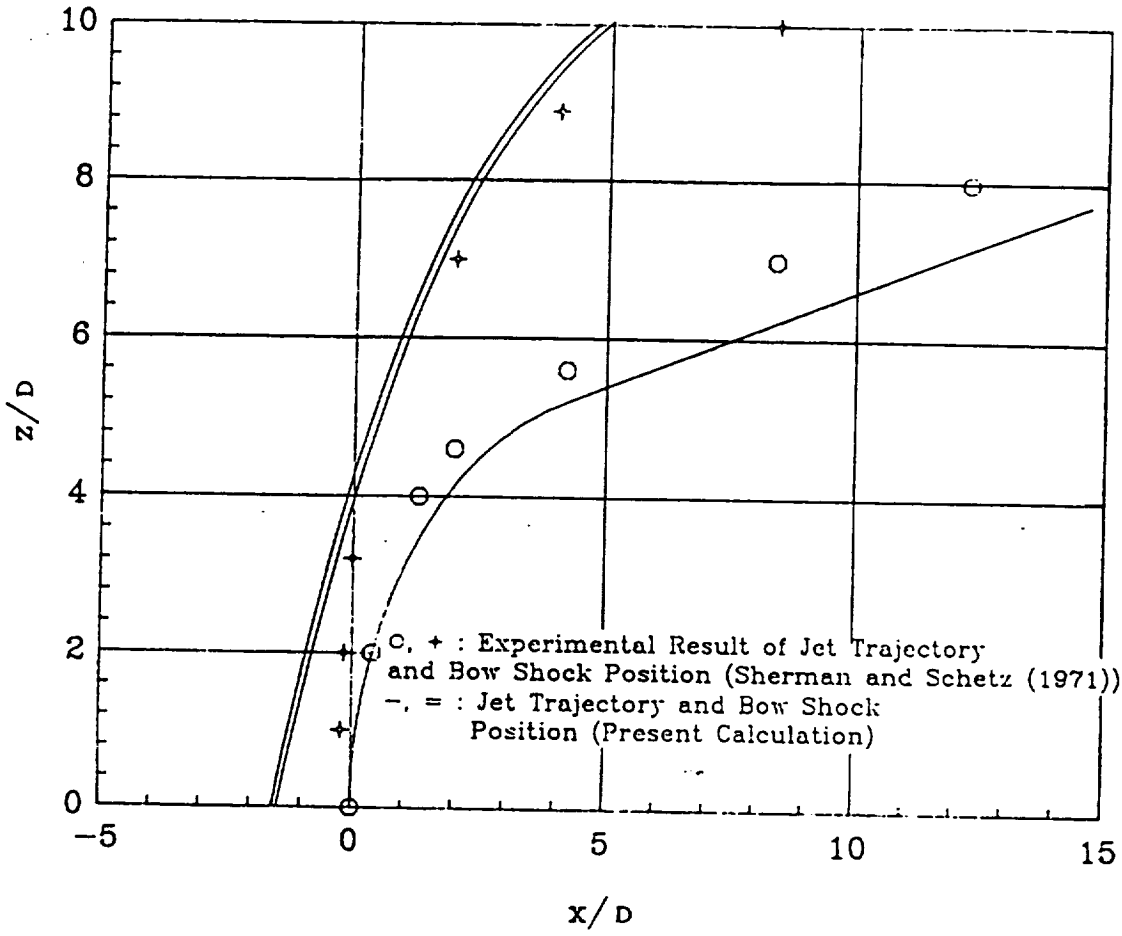

Figure 5b Computed jet trajectory for $M_\infty = 2.1, J = 6$, compared with experimental results (from Heister, et al.(1989)).

CHAPTER III

PREDICTION OF TRANSVERSE LIQUID JET BREAKUP

Considerable attention has been given to the physical process of transverse liquid jet breakup and its role in the control of the rate and/or completeness of combustion for many years (see Clark (1964), Sherman and Schetz (1971), Nejad and Schetz (1972), and Schetz, et al. (1980)). The jet breakup location divides the combustion process into two stages. Before breakup, the transverse liquid fuel jet evaporates and reacts with the oxidizer in the gas-phase boundary layer at the surface of a coherent, curved liquid column. This combustion process will be examined in next chapter. After breakup, the liquid fuel droplets interact with the gas stream (and, under some circumstances, each other), and burn either as individual particles or as droplet clusters (Faeth (1977)). Thus, the determination of jet breakup location is a first step in the overall understanding of combustion in the transverse liquid fuel jet.

In attempting to provide a reliable prediction for the breakup location in supersonic crossflow, we first consider the simple criterion that the liquid jet column fractures shortly behind the local sonic point, which was first observed by Schetz, et al. (1980). This criterion, which concerns only the properties of the inviscid external gas flow, has been shown to be effective in predicting the breakup location, without having to deal with complicated wave phenomena and surface instabilities in the liquid flowfield. The location of the local sonic point at the liquid surface is calculat-

ed here by two different analytical/numerical procedures. Using the model of Heister, et al. (1989) described in the previous chapter, the local sonic point is first determinated from the inviscid, compressible calculations using Godunov's (1961) numerical scheme. For purposes of comparison, a two-dimemsional blunt body model of the jet is also developed and used to predict the local sonic point. Predictions by both approaches are compared with experimental observations.

As an alternative breakup criterion to that of the local sonic point, we also explore a surface instability criterion concerning the dynamic interaction between surface tension and aerodynamic forces in this chapter. Comparison is also made here with experimental observations.

3.1 Calculation of the Local Sonic Point

3.1.1 Three-dimensional Approximation

In taking a slice of the transverse liquid fuel jet, whose trajectory has been determined by the previously described calculation, the external flow approaches the jet at a local effective Mach number $M=M_{\infty}\sin(\phi)$, where ϕ is the local angle of orientation of the jet (see Figure 1) and M_{∞} is the free stream Mach number. By computing the pressure distribution, velocity distribution, and the bow shock shape for the local external flow, incorporation of this information into mass and momentum balances along the jet allows estimation of the global gas properties for the entire three-dimensional flowfield.

The scheme developed by Godunov, et al. (1961) is used to compute the flow external to the liquid jet cross-section and boundary layer because of its inherent stability , its computational efficiency, and the fact that it performs well in domains where only a single shock is present. The scheme provides a first order accurate, explicit formulation of the two-dimensional Euler equations of gas dynamics written in conservative form. The numerical code, which is described in detail in Heister et al. (1989) and Heister (1987), is constructed in finite volume form and is able to accomodate arbitrary two-dimensional skewed cells. The boundary of the jet cross-section is assumed to be an ellipse, so that elliptic coordinates can be used to generate the grid. The assumption that the stagnation streamline for a vortex pair recirculation cell is very nearly elliptical is easily demonstrable.

To expand our locally two-dimensional solutions to the global three-dimensional flow properties for the determination of local sonic point, we must consider now the local axial velocity. In this stage, we are interested in the component of velocity that lies along the direction of the jet flow at its stagnation point. Because the component of velocity tangential to the bow shock (in the plane of the jet) is conserved, it is reasonable to approximate the local axial velocity just outside the jet as $v=U_\infty \cos\phi$. We can then compute the resultant Mach number in each grid cell along the jet by coupling the solution of the jet orientation to the numerical compressible flow solution. The local sonic point has thus been determined by this global Mach number distribution in a straight forward manner.

Figures 6a and 6b show the location of the local sonic point on the liquid fuel jet, as an indication of the breakup location, at different values of free stream Mach

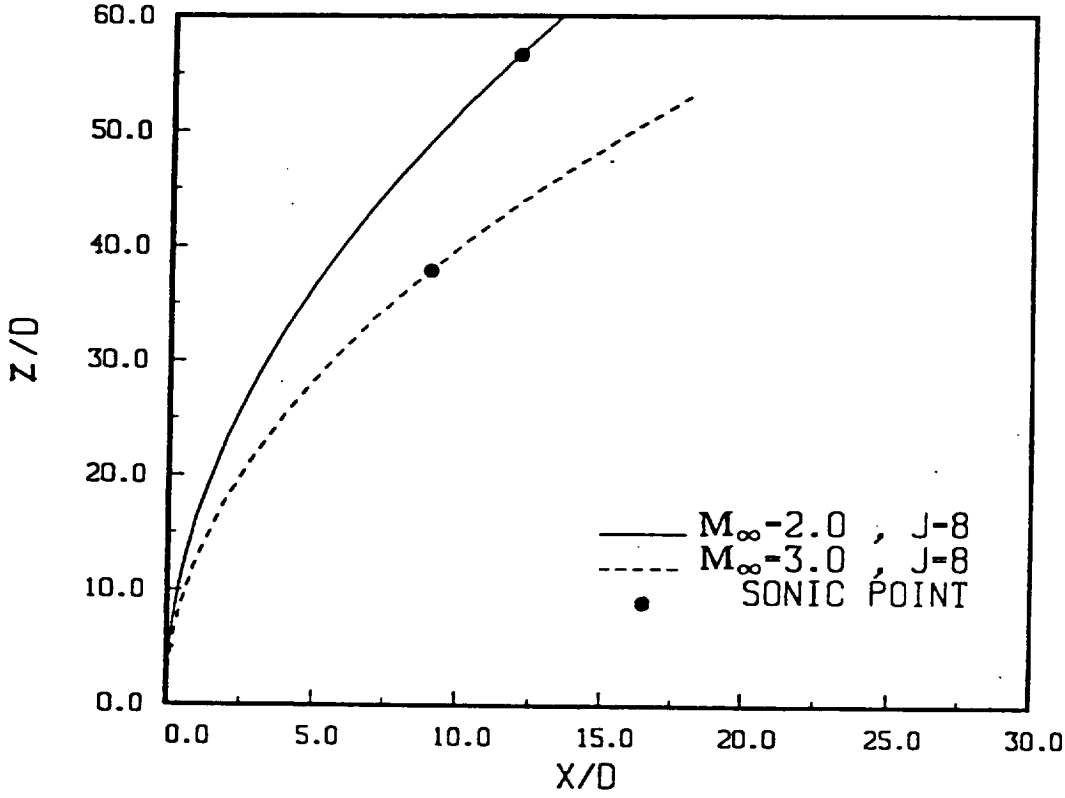

Figure 6a Computed local sonic point on the liquid jet for J=8.

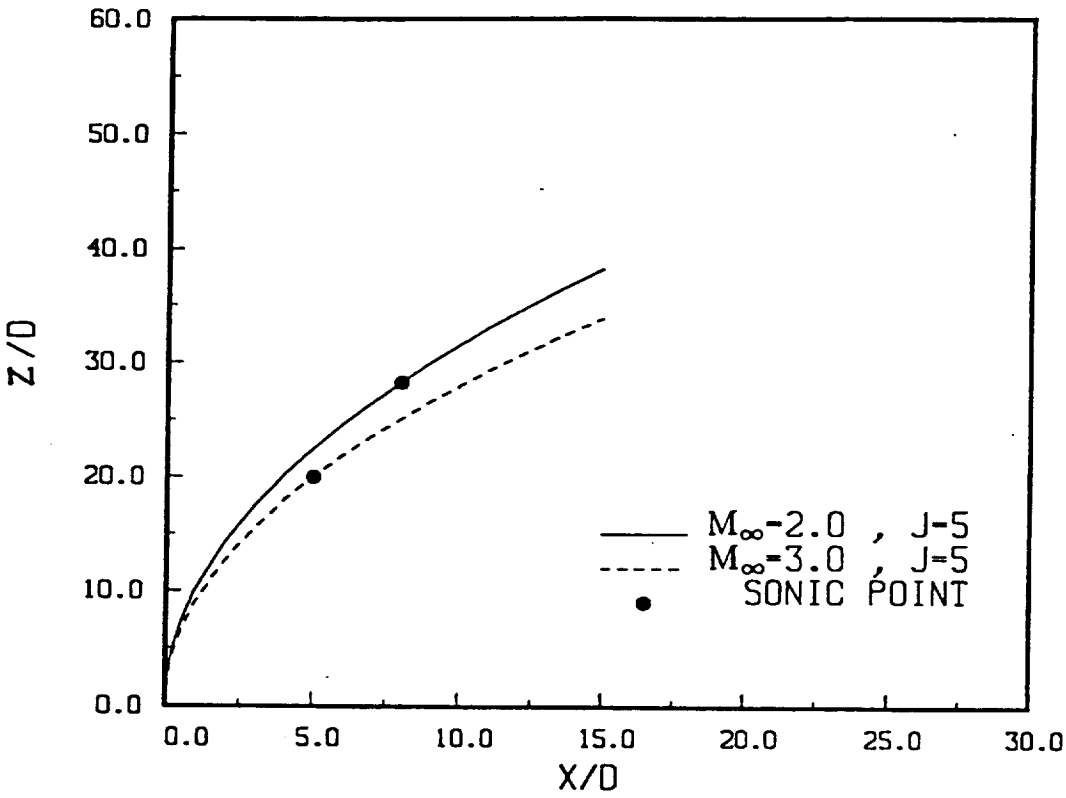

Figure 6b Computed local sonic point on the liquid jet for J=5.

number M_∞ and jet-to-crossflow momentum flux ratio $J \equiv \frac{\rho_j U_j^2}{\rho_\infty U_\infty^2}$. The breakup location ranges from 5 to 10 diameters downstream for $J = 5$, and from 8 to 13 for $J = 8$. The sonic point on the liquid jet occurs further downstream with increasing momentum flux ratio and decreasing upstream Mach number (see also Figures 7a and 7b). These correlations agree with previous investigators' conclusions (see Less and Schetz (1986) and Schetz, et al. (1980)), particularly in that the breakup occurs at roughly 10 jet diameters downstream of injection. This correspondence with experimental observation is further exemplified by plotting the local angle ϕ corresponding to the sonic point as a function of M_∞ (Figure 8). The angle ϕ corresponding to the sonic point ranges from about 50 degrees (for $M_\infty = 1.5$) to about 75 degrees (for $M_\infty = 3.5$), which is consistent with observations of breakup when the jet has turned by 25-30 degrees from the initial vertical. Because this general solution is dependent on momentum ratio, it is particularly useful in determining the breakup location when the jet trajectory is known. This figure again shows the tendency that the smaller the M_∞, the further downstream the sonic point.

3.1.2 Two-dimensional Approximation

To gain a deeper insight into the nature of modeling the transverse liquid jet and its sonic point, a two-dimensional blunt body model is also used in calculating the external gas flow properties. By assuming the jet shape to act as an effective two-dimensional blunt body to the upstream gas flow, the supersonic flowfield ahead of the body, including the sonic point, can be calculated again by the Godunov scheme used in previous calculation.

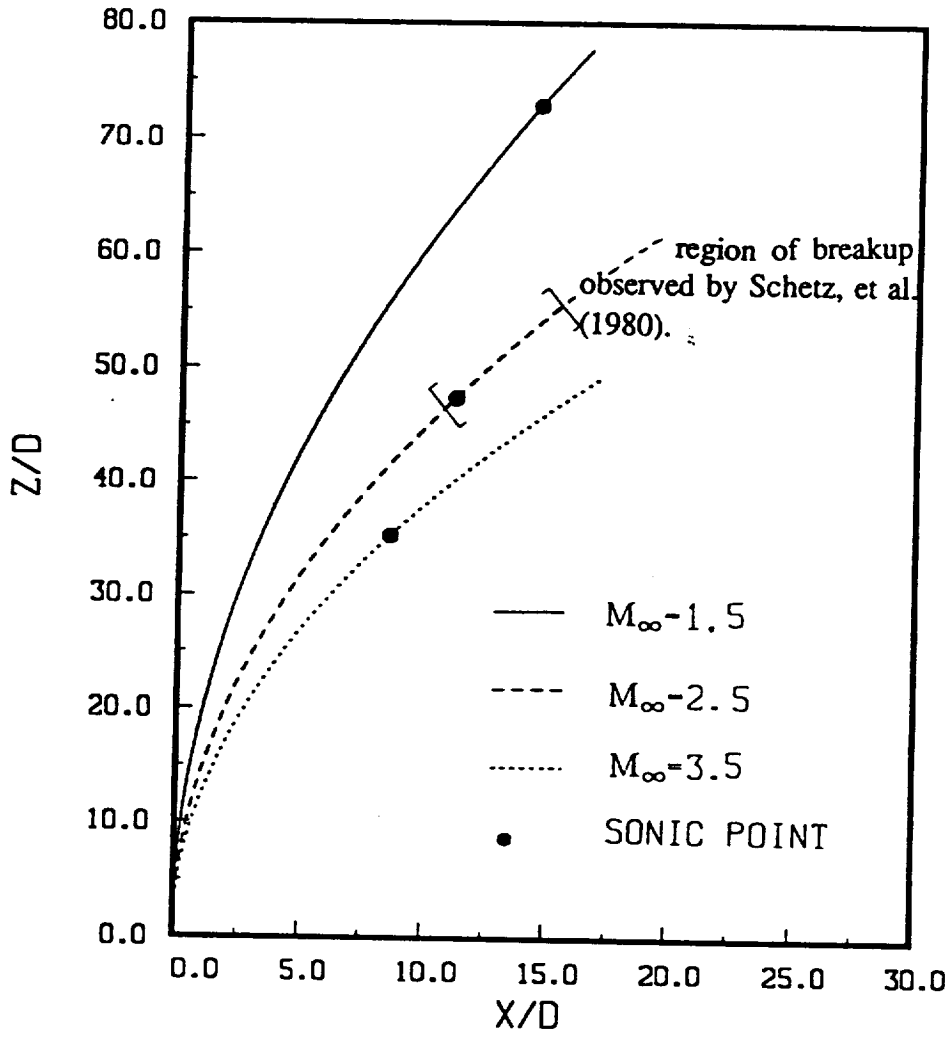

Figure 7a Computed local sonic point on the liquid jet for J=8.

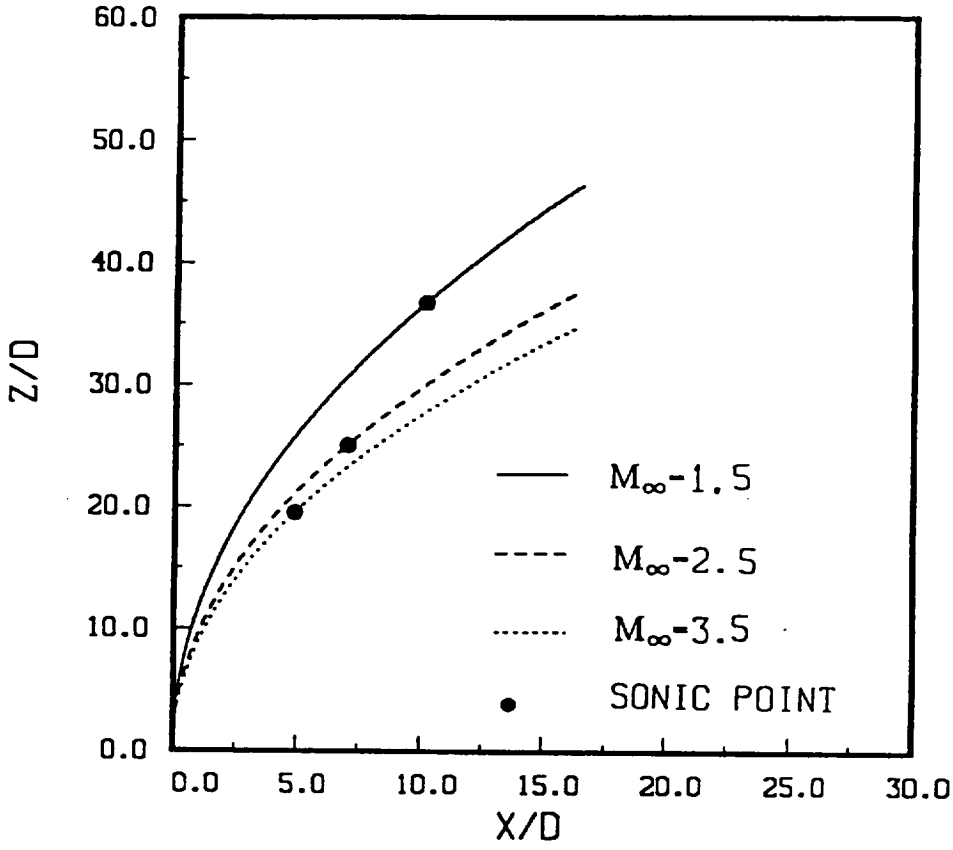

Figure 7b Computed local sonic point on the liquid jet for J=5.

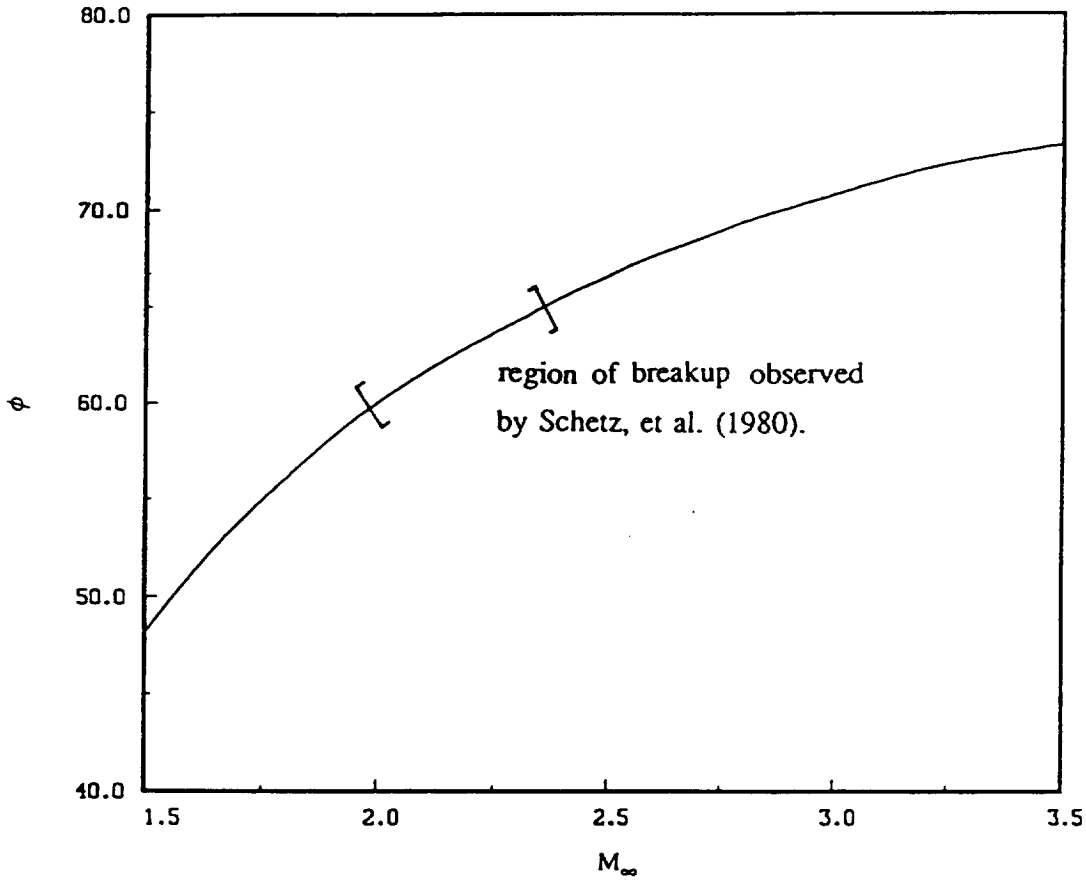

Figure 8 Angular orientation of transverse jet at its local sonic point as a function of upstream Mach number.

The numerical grid generation for this calculation is constructed by transforming the physical polar coordinate domain (r , θ_b) , where $r \geq R$ and $R(\theta_b)$ is the mathematical represention of the blunt body shape, to the computational domain (ξ_b , η_b) by

$$\begin{bmatrix} r \\ \theta_b \end{bmatrix} = \begin{bmatrix} (3\xi_b+1)R \\ \frac{\pi}{2}\eta_b \end{bmatrix} \tag{3.1}$$

This transformation is shown schematically in Figure 9. The domain of computation is from $\xi_b = 0$ (blunt body surface) to $\xi_b = 1$ ($r = 4R$, far beyond the bow shock location). The shape of the jet or the blunt body is calculated from the approximate solution of Heister, et al. (1989).

Figures 10a and 10b are two typical solutions of the two-dimensional supersonic external flow about the blunt body, with the bow shock shape and the local sonic line detailed. As compared with empirical data and calculations based on the approximate three-dimensional solution, both the bow shock and the local sonic point occurs significantly upstream of their experimentally observed locations. Clearly, these errors are caused by the neglect of the three-dimensional relieving effects actually present in this complex flowfield. While the model of Heister, et al. (1989) may only approximate these three-dimensional effects by taking two-dimensional slices of the jet cross-section, the model appears to reasonably represent enough of the important physics to be able to predict bow shock and sonic point locations accurately.

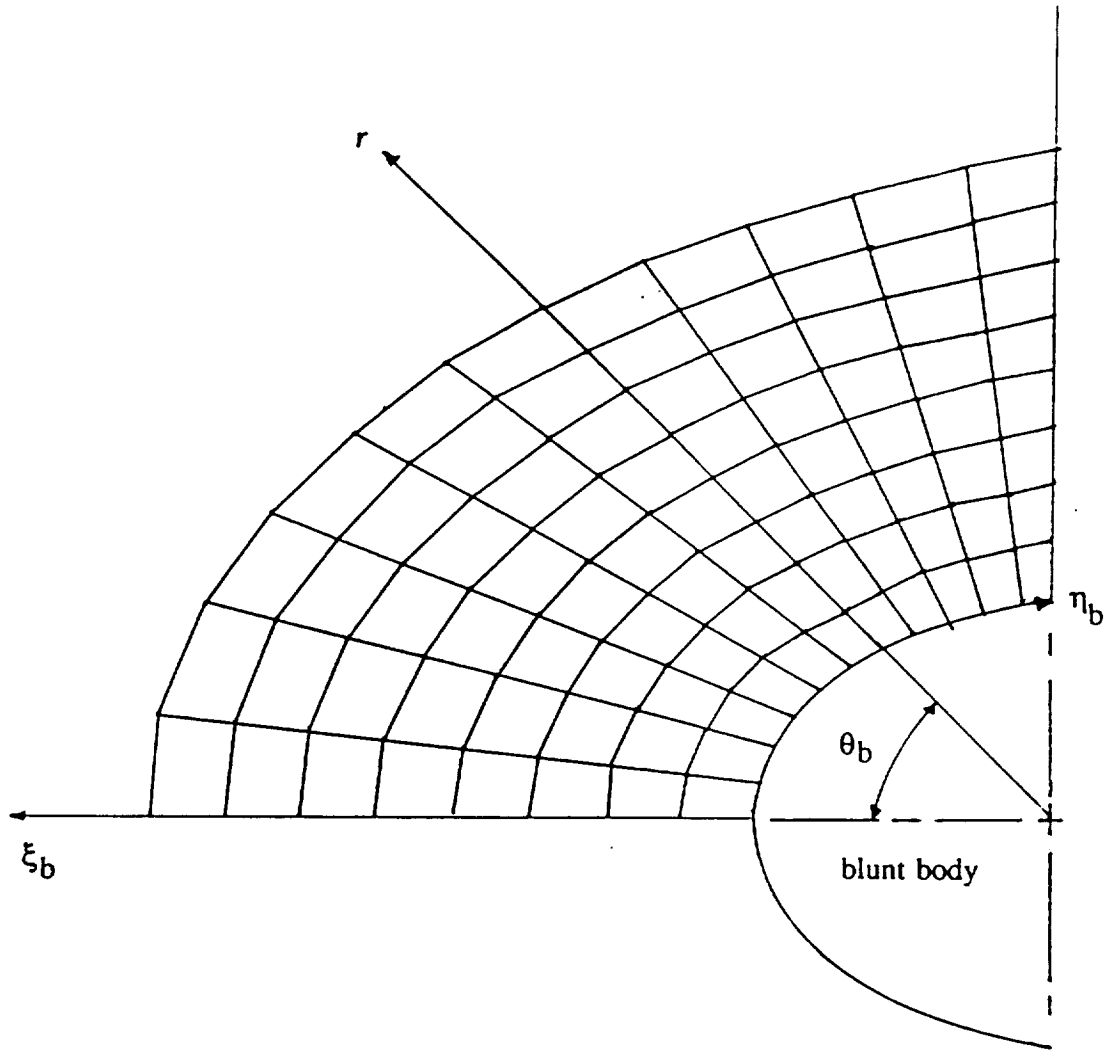

Figure 9 Grid generation for blunt body calculation.

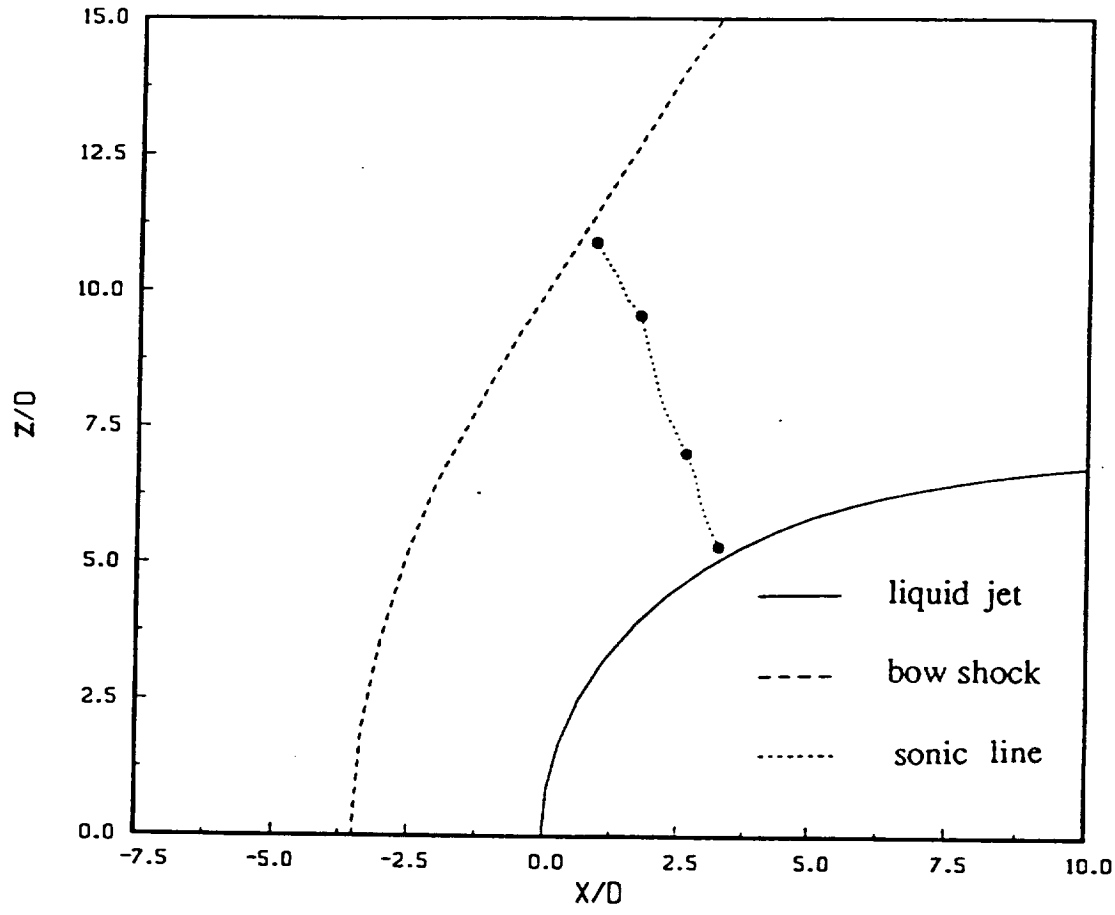

Figure 10a Computed local sonic point and bow shock shape for $J=5$ and $M_\infty = 3$.

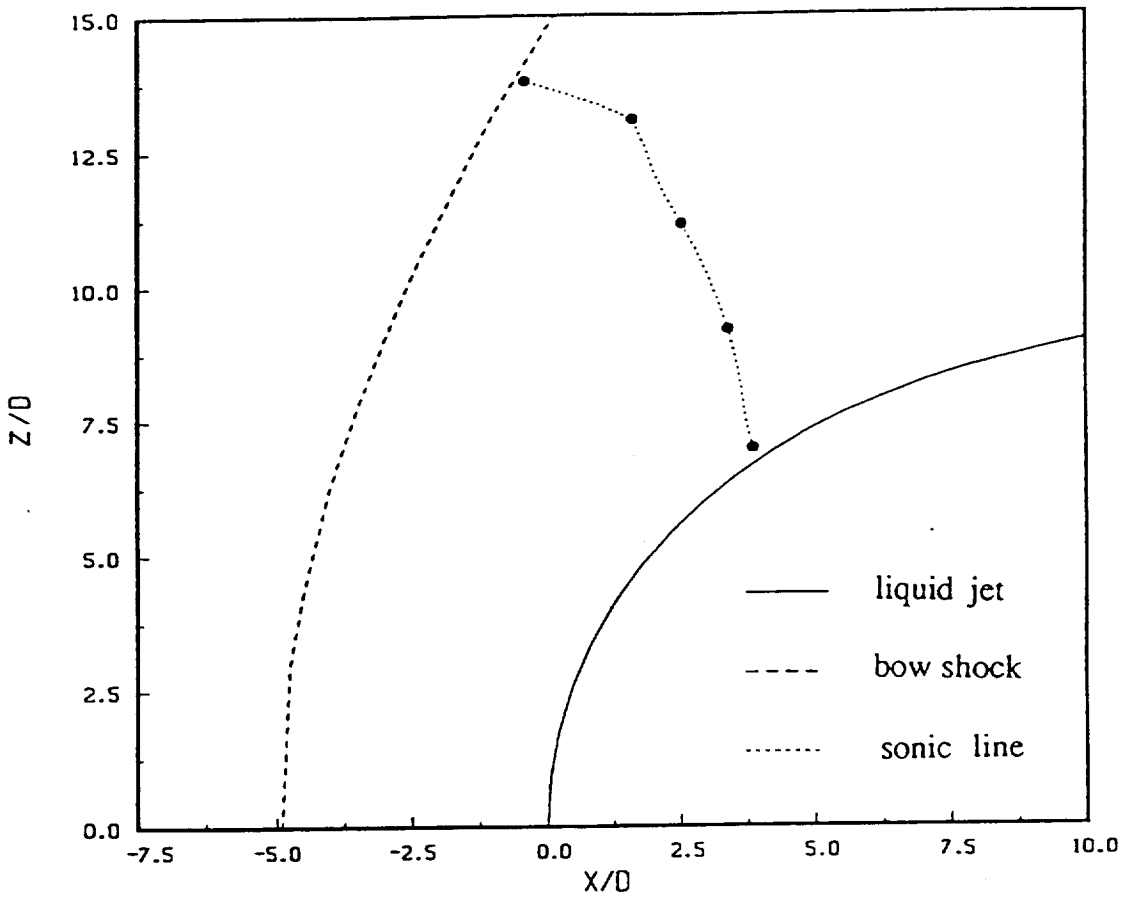

Figure 10b Computed local sonic point and bow shock shape for J =7 and $M_\infty = 3$.

3.2 Calculation of Stresses

The importance of the surface tension instability to the breakup process is examined in this section, as one other alternative to determine the transverse jet breakup location. In the experimental studies by Clark (1964), the author indicates that the breakup of a transverse liquid jet can be deduced from a consideration of the internal and external forces acting at the liquid interface. Contributing to the breakup process are the normal and tangential components of the aerodynamic force of the compressible gas acting at the liquid surface. The tangential component of stress, in particular, becomes very large further downstream of the injection point. Moreover, though the surface tension of the liquid tends initially to restore the liquid to its original cross-sectional shape, it actually, in the later stages of jet development, assists in the process of disintegration (Clark (1964)). Hence as a first-order estimate, the location where aerodynamic forces due to shear and surface tension are of the same order can be used as a criterion for determining the breakup location.

The present calculation focuses on the distribution of axial shear stresses at the liquid-gas interface along the jet trajectory, evaluated at the jet's local stagnation point, where the stresses are the most severe. This problem requires solution of the local gas and liquid phase velocity profiles simultaneously along the jet trajectory. For this type of two-phase flow problem, we consider a two-dimensional slice of the jet taken parallel to the centerline of the jet trajectory, intersecting the stagnation region along the jet. In view of solving for the axial shear stresses at the interface, this mathematical model serves well in simplifying the vector space and reasonably reproducing the most severe conditions for shear stress distribution.

The two-dimensional, steady momentum equation describing flow in the liquid phase boundary layer in the axial direction takes the form

$$u\frac{\partial u}{\partial s} = -\frac{1}{\rho}\frac{\partial p}{\partial s} + \nu_l \frac{\partial^2 u}{\partial y^2} \tag{3.2}$$

where s and y are the components parallel and normal to the jet trajectory, respectively, and ν_l is the local kinematic viscosity of the liquid. This *sy* coordinates is shown schematically in Figure 11. Furthermore, by applying Bernoulli's equation along the liquid jet trajectory, we have

$$U_0 \frac{dU_0}{ds} = -\frac{1}{\rho}\frac{dp}{ds} \tag{3.3}$$

where $U_0(s)$ is the local velocity within the liquid freestream. Equation (3.2) then reduces to

$$u\frac{\partial u}{\partial s} = U_0 \frac{dU_0}{ds} + \nu_l \frac{\partial^2 u}{\partial y^2} \tag{3.4}$$

and because of the symmetry at the centerline and the continuity of shear stresses at the interface, we write the boundary conditions as

$$y = 0 \quad , \quad \frac{\partial u}{\partial y} = 0$$

$$y = \frac{W}{2} \quad , \quad \mu_g \frac{\partial u}{\partial y} = \mu_l \frac{\partial u}{\partial y}$$

Here W is twice the semi-minor axis of the elliptical jet cross-section, μ_g is the local dynamic viscosity of the gas, and μ_l is the local dynamic viscosity of the liquid.

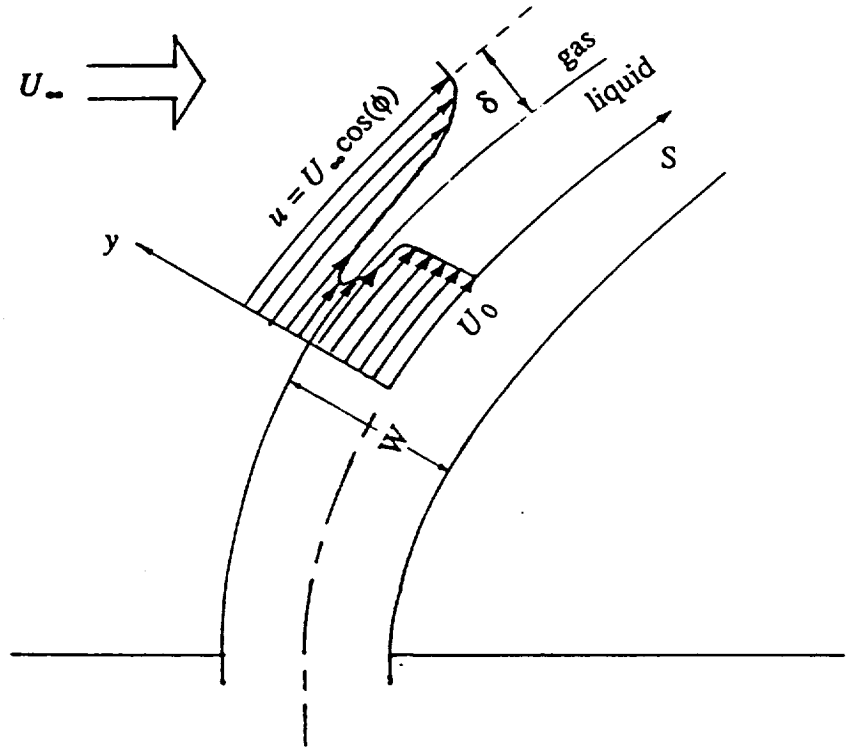

Figure 11 Schematic of *sy*-coordinates along jet trajectory.

Following the same analytical process for the liquid-phase flow, the governing equation for the gas-phase layer is written as

$$u\frac{\partial u}{\partial s} = -\frac{1}{\rho}\frac{\partial p}{\partial s} + \nu_g \frac{\partial^2 u}{\partial y^2} \tag{3.5}$$

with boundary conditions

$$y = \frac{W}{2}\ , \qquad \mu_g \frac{\partial u}{\partial y} = \mu_l \frac{\partial u}{\partial y}$$

$$y = \frac{W}{2} + \delta_g\ , \quad u = U_\infty \cos(\phi)$$

where ν_g is the local kinematic viscosity of the gas, δ_g is gas boundary layer thickness, and U_∞ is infinite free stream velocity. The pressure distribution at the stagnation point along the jet trajectory is derived from shock dynamics and can be written as

$$p = p_\infty (1+0.2M^2)^{3.5}\ (1.167M^2 - 0.167)^{-2.5}\ \left(\frac{1}{1.2M^2} + 0.167\right)^{-3.5}$$

where the local effective Mach number upstream of the bow shock $M = M_\infty \cos(\phi)$.

In attempting to solve the governing equations simultaneously, we first non-dimensionize equations (3.4) and (3.5) using the initial liquid velocity U_j at the injection point and twice the semi-minor axis W, to get

$$\bar{u}\frac{\partial \bar{u}}{\partial \bar{s}} = \bar{U}_0 \frac{\partial \bar{U}_0}{\partial \bar{s}} + \frac{1}{\mathrm{Re}_l}\frac{\partial^2 \bar{u}}{\partial \bar{y}^2} \tag{3.6}$$

$$\bar{u}\frac{\partial \bar{u}}{\partial \bar{s}} = -\frac{\partial \bar{p}}{\partial \bar{s}} + \frac{1}{\mathrm{Re}_g}\frac{\partial^2 \bar{u}}{\partial \bar{y}^2} \tag{3.7}$$

where $\bar{s} \equiv s/W$, $\bar{y} \equiv y/W$, $\bar{u} \equiv u/U_j$, $\bar{U}_0(\bar{s}) \equiv U_0(\bar{s})/U_j$, $\bar{p} \equiv p/\rho U_j^2$, and where the jet Reynolds number $\mathrm{Re}_l = \dfrac{U_j W}{\nu_l}$, and the "gas" Reynolds number Re_g is defined here as $\dfrac{U_j W}{\nu_g}$. The non-dimensionized boundary conditions reduce to:

$$\bar{y} = 0, \qquad \frac{\partial \bar{u}}{\partial \bar{y}} = 0$$

$$\bar{y} = 0.5, \qquad \mu_g \frac{\partial \bar{u}}{\partial \bar{y}} = \mu_l \frac{\partial \bar{u}}{\partial \bar{y}}$$

$$\bar{y} = 0.5 + \frac{\delta_g}{W}, \quad \bar{u} = \frac{U_\infty}{U_j} \cos(\phi)$$

By using backward discretization based on the Crank-Nicolson scheme, we can transform the governing differential equations into tridiagonal difference equations. The crucial part of this numerical procedure involves handling the interface condition. By introducing imaginary points into the opposite phase layer for both gas-phase and liquid-phase flow at the interface, we are able to satisfy the interface boundary condition. After tedious linear algebraic operations, the governing equations reduce to the final matrix equation $Au=b$, where the matrix A takes the form

$$\begin{bmatrix} 1 & 0 & 0 & 0 & 0 \\ \dfrac{-1}{\mathrm{Re}_g hu_{ij}} & 1+\dfrac{2}{\mathrm{Re}_g hu_{ij}} & \dfrac{-1}{\mathrm{Re}_g hu_{ij}} & 0 & 0 \\ 0 & < \dfrac{-1}{\mathrm{Re}_l hu_i^*} \quad \dfrac{2}{C_1+C_2}, & 1+\dfrac{2}{\mathrm{Re}_l hu_i^*}, & \dfrac{-1}{\mathrm{Re}_l hu_i^*} \quad \dfrac{2C_2}{C_1+C_2} > & 0 \\ 0 & 0 & \dfrac{-1}{\mathrm{Re}_l hu_{ij}} & 1+\dfrac{2}{\mathrm{Re}_l hu_{ij}} & \dfrac{-1}{\mathrm{Re}_l hu_{ij}} \\ 0 & 0 & 0 & \dfrac{-2}{\mathrm{Re}_l hu_{in}} & 1+\dfrac{2}{\mathrm{Re}_l hu_{in}} \end{bmatrix}$$

where h is the step size of discretization and u_{ij} is velocity at each grid point, and where the terms inside the brackets < > are the terms in the final interface equation, where u_i^* is the interface velocity, and $C_1 = \dfrac{\mathrm{Re}_g}{\mathrm{Re}_l}$, $C_2 = \dfrac{\mu_l}{\mu_g}$. The axial velocity profiles along the jet trajectory are obtained by solving the above matrix equation iteratively through out the entire flowfield.

Figures 12a-e display the local velocity profiles of the liquid and gas phase boundary layers along the jet trajectory at different axial locations. In the range of $0 \le \bar{y} \le 0.5$,the profile expresses the variation of liquid-phase velocity, while in the range $0.5 \le \bar{y} \le 0.53$,the profile represents part of the gas-phase boundary layer velocity. Initially, the axial interface velocity increases rapidly from zero at the injection point in the first few diameters downstream, and then it gradually goes to its maximum ($\approx 0.63U$) at around $\bar{s} = 9$. From the velocity profile, as we have expected, the liquid and gas viscous layers are relatively thin. This is different from the transverse gas jet, whose internal axial velocity profile changes significantly throughout the entire flowfield during the penetration process. The reason that the viscous stresses are confined to a thin layer in the liquid jet problem is that the kinematic viscosity of the

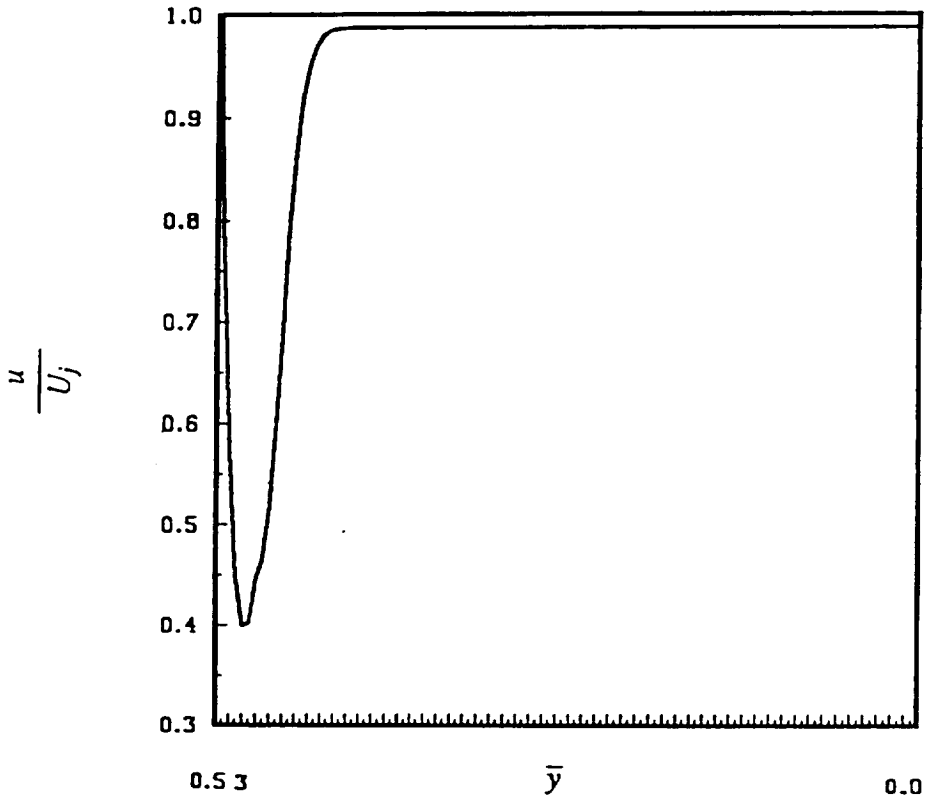

Figure 12a Computed axial velocity distribution at $\bar{s}$=1.

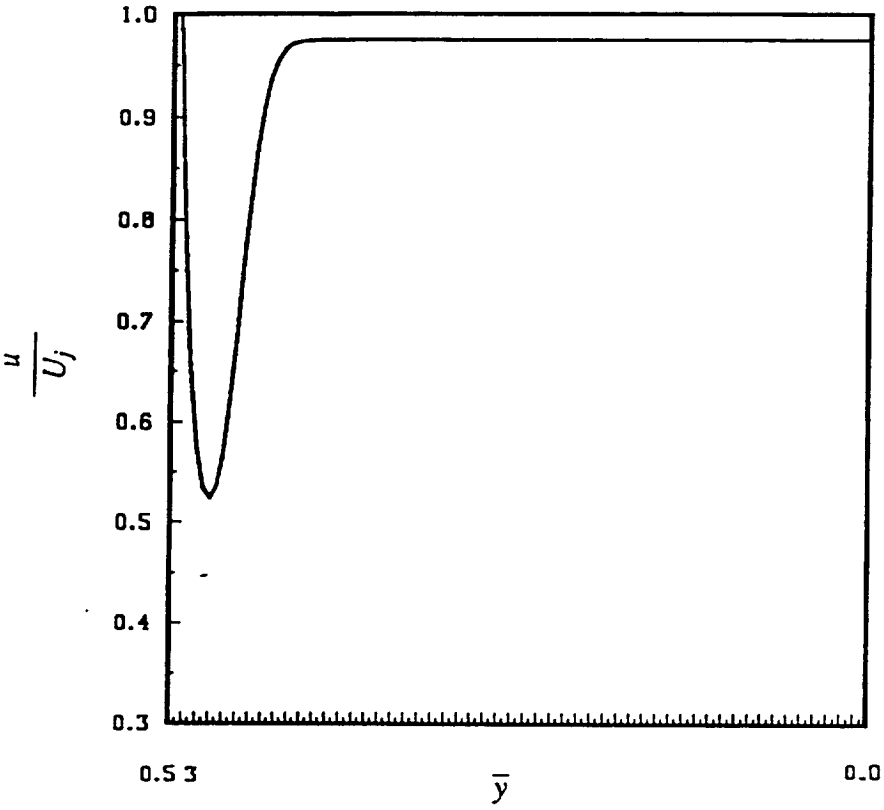

Figure 12b Computed axial velocity distribution at $\bar{s}$=2.

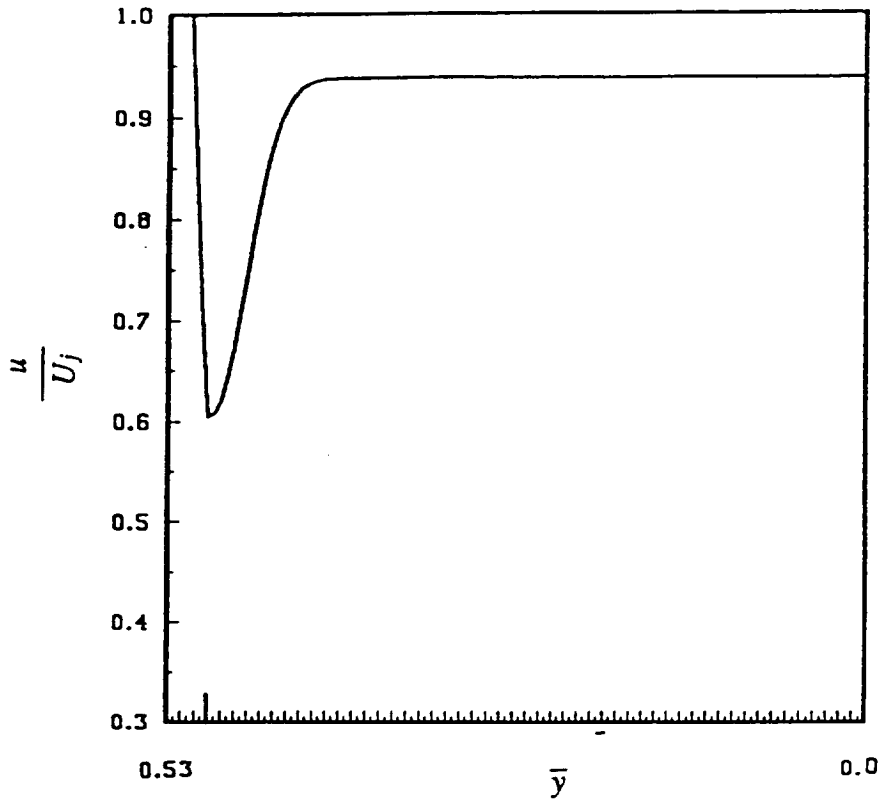

Figure 12c Computed axial velocity distribution at $\bar{s}$=5.

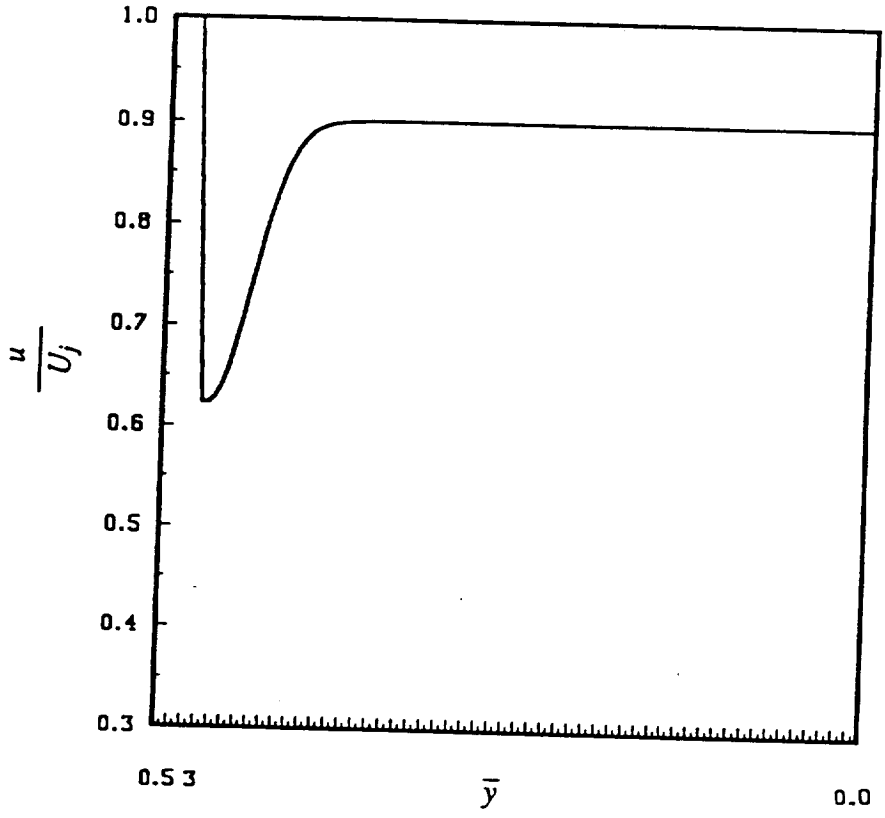

Figure 12d Computed axial velocity distribution at $\bar{s}$=9.

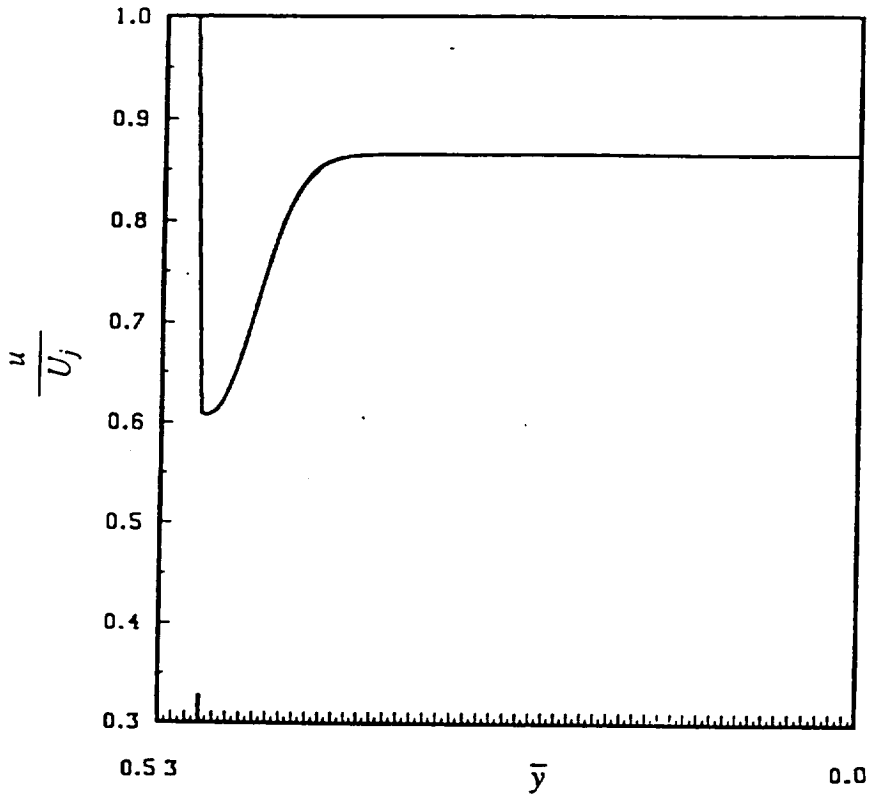

Figure 12e Computed axial velocity distribution at $\bar{s}$=10.

liquid is one to two orders of magnitude lower than that of the gas. These velocity profile characteristics for the present model are consistent with those from general boundary layer theory. The error that arises due to neglect of terms of the order $\nu\frac{\partial u}{\partial y}$ is well within 5 percent.

Figures 13ab details the nondimensional interface shear stresses along the jet trajectory evaluated at the local jet stagnation point. At the jet orifice, resulting from the singularity of the axial component of the gas velocity at the injection point and the wall effect of nozzle, the shear stress is somewhat less than zero. But as soon as the jet turns while penetrating the crossflow, the shear stress increases significantly and monotonically due to the increasing blowing strength.

From the computed shear stress acting at the liquid interface, together with the effective surface tension stress $\frac{2\sigma}{W}$, the concept of transverse jet breakup first proposed by Sherman and Schetz (1971) and Nejad and Schetz (1972) can be explored. The location at which both stresses are of the same order (the so called "tension point") may indicate the beginning of the breakup process. Figures 14 and 15 display this "tension point" together with the previously determined sonic point along the jet trajectory. For higher momentum flux ratios, the "tension point" tends to occur a few diameters upstream of the sonic point, which lies closer to the actual breakup locations indicated by Schetz, et al. (1980). The "tension point" does not appear to vary significantly with momentum flux ratio, and very little with crossflow Mach number. This is consistent with the observation that the shear stress distribution does not vary significantly with M_∞ and J (see Figures 13ab). The estimation of the sonic point, however, inherently includes the alteration in the jet trajectory with different

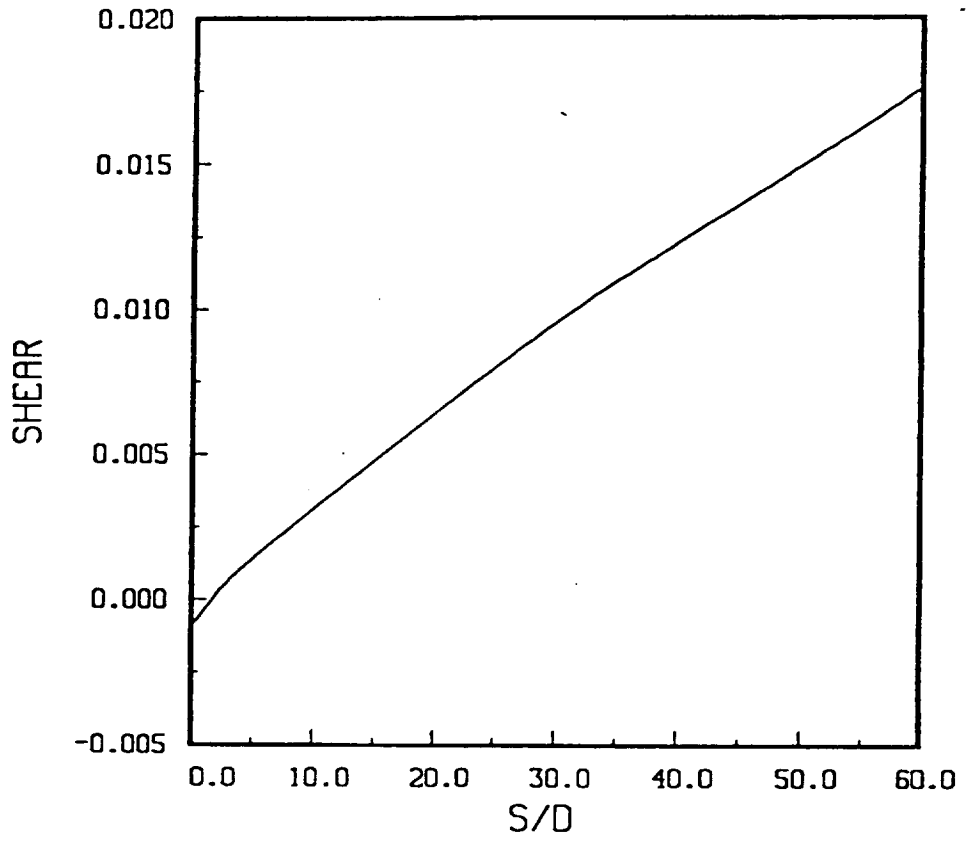

Figure 13a Computed variation of shear stess evaluated at stagnation point along jet trajectory for M_∞=3,J=8.

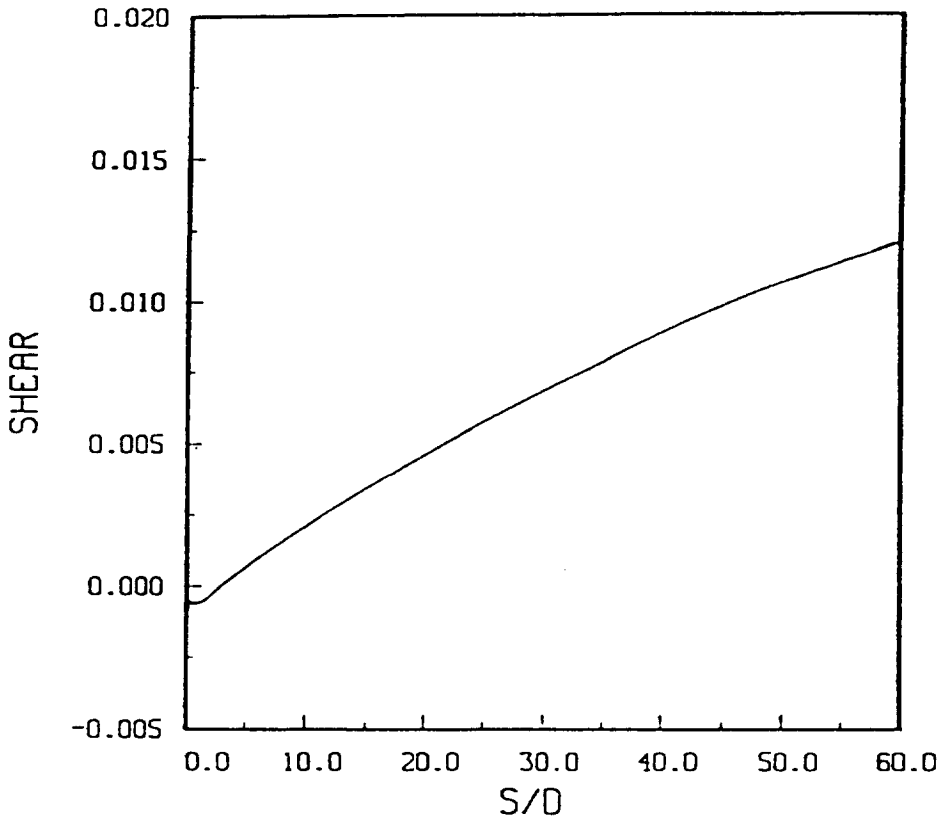

Figure 13b Computed variation of shear stess evaluated at stagnation point along jet trajectory for M_∞=2,J=5.

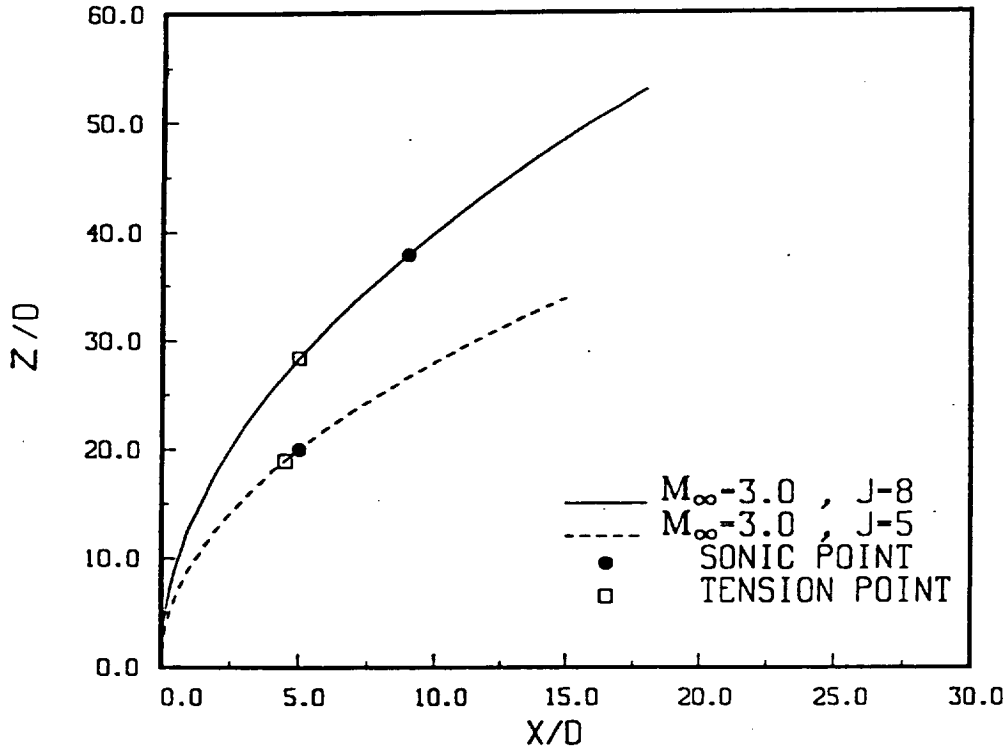

Figure 14 Computed local sonic point and tension point on the liquid jet at $M_\infty = 3$.

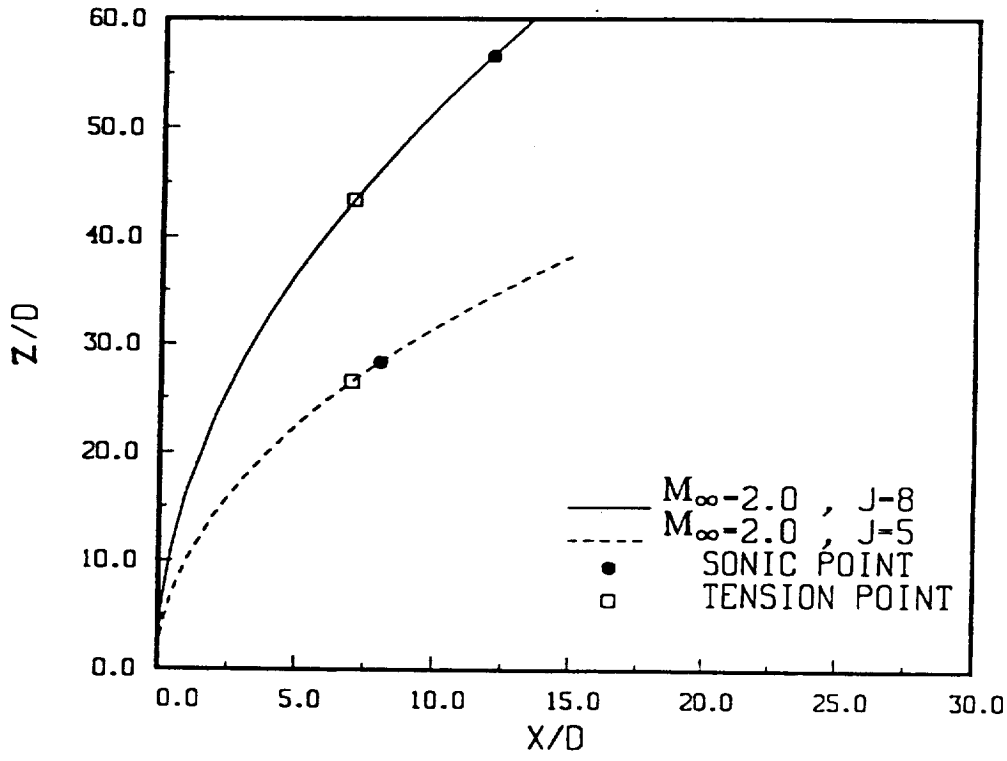

Figure 15 Computed local sonic point and tension point on the liquid jet at $M_\infty = 2$.

input values of M_∞ and J, so that the sonic point varies more significantly with these input variables.

3.3 Discussion

The prediction of the liquid transverse jet breakup location has been estimated using the model of Heister, et al. (1989) and the criteria of the local sonic point and surface tension shear stress balance. Generally, the sonic point criterion is more successful in predicting the breakup location as observed by experimental researchers (Schetz, et al. (1980)), although at lower jet-to-crossflow momentum flux ratios, the "tension point" criterion also may be reasonable. While the present approach certainly is not the "final word" in the study of liquid transverse jet breakup in a supersonic stream, it does provide a computationally inexpensive (one minute on an IBM 3090-600s) means of estimating the breakup point. The calculation also estimates the limit for the applicability of coherent liquid jet models (e.g., Adelberg (1967), Catton, et al. (1968), Heister, et al. (1989), and Nguyen and Karagozian (1990)).

CHAPTER IV

THE BURNING LIQUID JET WITH FINITE RATE CHEMISTRY

Studies of combustion in the gas phase boundary layer of the transverse liquid jet with an infinitely fast chemical reaction rate have been completed by Nguyen (1989) for low subsonic crossflow. In this study, sharp discontinuities in the gradients of mass fractions and temperature across the diffusion flame reflect a very thin flame front, and allow prediction of fuel consumption rates without having to deal with the complex chemical kinetics required to represent the reaction more accurately.

In the limit of fast chemistry, the energy and species equations are simplified to the equilibrium case with only a chemical source term at the flame front. In the solution by Nguyen (1989) (also described in Nguyen and Karagozian (1990)), the gaseous boundary layer equations are reduced to a set of coupled ordinary differential equations via the Levy-Lees and Howarth-Dorodnitzyn transformations (see Lees (1956)) to characterize the effects of chemical reaction in the compressible boundary layer. Solution of the equations allows calculation of velocity, species, and and temperature profiles in the gas phase, and evaluation of mass loss at the liquid surface with and without the combustion process. In order to predict more complex combustion phenomena such as ignition, however, it becomes necessary to represent the reaction using finite rate chemistry.

A number of theoretical and numerical studies have reported on the fundamental problem of chemical reactions in the gas phase boundary layer adjacent to a liquid fuel surface. A thorough study by Chung (1965) for chemically reacting non-equilibrium boundary layers covers both the surface reaction case and the gas-phase reaction case using the methods of nonsimilar and self-similar solutions. The same type of flow situation also occurs in the boundary layer adjacent to a burning liquid fuel droplet in a convective flowfield (studied, for example, by Saitoh and Nagano (1980)). In these studies, finite rate chemistry allows more accurate solution of the reaction zone.

In the present work, we consider a one step irreversible Arrhenius second order equation for the finite rate chemical reaction across the diffusion flame. This approach, though requiring more complexity in the computational method, will make it possible to study detailed reaction mechanisms, particularly those associated with ignition and, possibly, extinction. In the study of ignition and flame spread by Kashiwagi and Summerfield (1972),the authors have shown that, in convective ignition, an exothermic gas-phase reaction rather than an exothermic surface reaction controls ignition. They use a maximum in the integrated value of reaction rate through the gas-phase boundary layer as a criterion which is successful in predicting ignition characteristics. This approach is used in the present analysis to predict fuel jet ignition, again, in low subsonic crossflow only. The incorporation of finite rate chemistry into the analysis also allows more accurate calculations of evaporation rate to be carried out, in addition to flame temperature, mass fraction distributions, and reaction rates.

4.1 Development of equations

For a homogeneous, finite rate chemical reaction in the boundary layer, assuming a one step irreversible Arrhenius reaction with a large activation energy E_a (see Williams (1985)), the molar rate of consumption of the fuel per unit volume is given by

$$\frac{1}{\alpha}\frac{dC_o}{dt} = \frac{dC_F}{dt} = \frac{\rho^2}{M_o M_F} Y_o Y_F A_r \exp\left[\frac{-E_a}{R_u T}\right]$$

for the reaction $\alpha [O_2] + [F] \rightarrow [P]$. Here $[O_2]$, $[F]$, and $[P]$ represent oxidizer, fuel, and combustion products, respectively, α represents the oxidizer-fuel stoichiometric ratio, C_o and C_F are the molar concentrations of oxidizer and fuel respectively, R_u represents the universal gas constant, M_o and M_F are molar weights of oxidizer and fuel respectively, A_r represents frequency coefficient of Arrhenius equation, and Y_o and Y_F are mass fractions of oxidizer and fuel respectively. Furthermore, we can write the oxidizer and fuel mass consumption rate as

$$\omega_o = \frac{\alpha\rho^2}{M_F} Y_o Y_F A_r \exp\left[\frac{-E_a}{R_u T}\right] \tag{4.1}$$

$$\omega_F = \frac{\rho^2}{M_o} Y_o Y_F A_r \exp\left[\frac{-E_a}{R_u T}\right] \tag{4.2}$$

The steady state governing equations for gaseous chemically reacting laminar boundary layers can then be deduced from the standard conservation equations for multicomponent reacting systems:

Continuity

$$\frac{\partial(\rho u)}{\partial x} + \frac{\partial(\rho v)}{\partial y} = 0 \tag{4.3}$$

Momentum

$$u\frac{\partial u}{\partial x} + v\frac{\partial u}{\partial y} = -\frac{1}{\rho}\frac{\partial p}{\partial x} + \frac{1}{\rho}\frac{\partial}{\partial y}(\mu\frac{\partial u}{\partial y}) \tag{4.4}$$

Species

$$u\frac{\partial Y_i}{\partial x} + v\frac{\partial Y_i}{\partial y} = D\frac{\partial^2 Y_i}{\partial y^2} - \frac{\omega_i}{\rho} \tag{4.5}$$

Energy

$$u\frac{\partial T}{\partial x} + v\frac{\partial T}{\partial y} = \frac{u}{C_p\rho}\frac{\partial p}{\partial x} + \frac{1}{C_p\rho}\frac{\partial}{\partial y}(\lambda\frac{\partial T}{\partial y}) + \frac{Q}{C_p}\frac{\omega_F}{\rho} + \frac{\mu}{C_p\rho}(\frac{\partial u}{\partial y})^2 \tag{4.6}$$

$$+ \frac{1}{C_p}\sum D\,(\frac{\partial Y_i}{\partial y})(\frac{\partial h_i}{\partial y})$$

where the enthalpy of species i, h_i, is defined to include the energy of formation, in the form

$$h_i = \int_0^T C_{pi}\,d\,T + h_i^0$$

In these equations, C_p, λ, D, and Q are the specific heat of the gas mixture at constant pressure, the thermal conductivity of the mixture, the coefficient of mass diffusion of the fuel in to the oxidizer, and heat of reaction per unit mass of fuel, respectively. Implicit in the above equations are such simplifying assumptions as the Fick's law of diffusion, constant specific heat, and constant thermal conductivity, in addition to the equation of state, $\rho T = \rho_e T_e$ (where e represents the external flow).

Following the customary boundary layer practice, we shall first investigate the possibility of obtaining a self-similar solution. For this purpose, we have to transform the governing equations and boundary conditions from (x , y) coordinates to (ξ , η) coordinates. Following the Levy-Lees transformation described by Chung (1965) and Kou (1986), we define

$$\eta = \frac{U_e}{\sqrt{2\xi}} \int_0^y \rho \, dy$$

where

$$\xi = \int_0^x \rho_e \mu_e U_e dx$$

The continuity equation (4.3) is automatically satisfied by introducing the stream function ψ, which is defined by the usual compressible relations

$$\rho u = \frac{\partial \psi}{\partial y}$$

$$\rho v = -\frac{\partial \psi}{\partial x}$$

Defining a nondimensional stream function F as

$$F(\eta) \equiv \frac{\psi}{\sqrt{2\xi}}$$

we then have

$$F_\eta = \frac{u}{U_e} \tag{4.7}$$

representing the nondimensional velocity distribution within the boundary layer, and

$$\rho v = \frac{\rho_e \mu_e U_e}{\sqrt{2\xi}} \eta F' - \frac{\rho_e \mu_e U_e}{\sqrt{2\xi}} F \tag{4.8}$$

representing vertical momentum convection.

By assuming $\rho\mu = \rho_e \mu_e =$ constant throughout the flow field, the conservation equations of momentum, species, and energy are thus transformed into: Momentum

$$F''' + FF'' + \beta[\theta - F'^2] = 0 \tag{4.9}$$

Species

$$\frac{1}{Sc} Y_i'' + FY_i' = \Delta_1 \frac{\alpha Y_o Y_F}{M_F} \frac{1}{\theta} \exp\left[\frac{-A_E}{\theta}\right] \tag{4.10}$$

Energy

$$\frac{1}{Pr}\theta'' + F\theta' - \Delta_2 \beta F'\theta + \frac{1}{LePr} \sum Y_i'\theta' = \tag{4.11}$$

$$= -\Delta_2 F''^2 - \Delta_1 \Delta_3 \frac{Y_o Y_F}{M_o} \frac{1}{\theta} \exp\left[\frac{-A_E}{\theta}\right]$$

where

$$\theta = \frac{T}{T_e}$$

$$A_E = \frac{E_a}{R_u T_e}$$

$$\Delta_1 = \frac{2\xi}{\mu \rho^2 U_e^2}$$

$$\Delta_2 = \frac{U_e^2}{C_p T_e}$$

$$\Delta_3 = \frac{Q}{C_p T_e}$$

β in equation (4.9) is called the "pressure gradient parameter" defined by

$$\beta = \frac{2\xi}{U_e}\frac{dU_e}{d\xi} \tag{4.12}$$

where ξ is the transformed distance along the elliptical surface (x coordinate), measured from the stagnation point. In the above equations, the Schmidt number $Sc = \frac{\mu}{\rho D}$, Prandtl number $Pr = \frac{C_p \mu}{\lambda}$, and Lewis number $Le = \frac{\lambda}{\rho D C_p}$ are assumed constant. The corresponding boundary conditions for the present problems are

$$\eta = 0: \; F' = \Gamma_s, \quad F = F_w, \quad Y_o = 0, \quad Y_F = Y_{Fw}, \quad \theta = \frac{T_w}{T_e}$$

$$\eta \to \infty: \; F' \to 1, \quad Y_o \to 1, \quad Y_F \to 0, \quad \theta \to 1$$

where Γ_s is the effective vortex strength which characterizes the surface flow along the jet cross-section boundary (see Nguyen and Karagozian (1990)).

The boundary layer equations (4.9)-(4.11) still cannot be solved since the boundary conditions involve two unknowns, namely, F_w, the value of the function F at the liquid surface, and Y_{Fw}, the fuel mass fraction at the surface. By assuming that the jet cross-section boundary is impermeable to the gaseous flow, however, the value of F_w is the measure of the evaporation rate, so that Y_{Fw}, in turn, depends upon the heat transfer rate across the liquid-gas interface. By considering the equation (4.8)

and the interface mass-flux balance of fuel,

$$(\rho D\frac{\partial Y_F}{\partial y})_w = (\rho v)_w\,[Y_{Fw+} - Y_{Fw-}] \tag{4.13}$$

the values of F_w and Y_{Fw} can be found to take the form

$$F_w = -B_0\theta'_w$$

$$Y_{Fw} = \frac{B_0}{1+B_0}$$

where

$$B_0 = \frac{C_p(T_e - T_w) + \alpha Q}{Q_l}$$

and Q_l is the effective latent heat of vaporization of fuel.

Thus, the values of F_w and Y_{Fw} are uniquely determined by the free stream conditions, the effective latent heat of vaporization of the fuel, the local temperature at the liquid-gas interface, and the wall temperature gradient.

4.2 Numerical procedure

In order to attempt a solution to the sytem of equations in the previous section, it is necessary first to reduce the third-order nonlinear ordinary differential equation (4.9). By introducing the new dependent variable f, defined by

$$f \equiv F'$$

equation (4.9) becomes

$$f'' + Ff' + \beta(\theta - f^2) = 0 \tag{4.14}$$

The standard Newton-Kantorovich procedure is then taken to quasilinearize both equations (4.14) and (4.11). The general nonlinear terms are linearized using the Frechet-Taylor expansion. We finally arrive at a solvable form for equation (4.14),

$$f'' + Ff' - 2\beta f^* f = -\beta(\theta + f^{*2}) \tag{4.15}$$

and the linearized terms

$$\frac{1}{\theta}\exp(\frac{-A_E}{\theta}) = \left[(\frac{2}{\theta} - \frac{A_E}{\theta^2})\exp(\frac{-A_E}{\theta})\right]^* + \left[(\frac{A_E}{\theta^3} - \frac{1}{\theta^2})\exp(\frac{-A_E}{\theta})\right]^* \theta \tag{4.16}$$

for the chemical source term in equation (4.11), where the superscription * denotes the previous iteration values.

By discretizing equations (4.10), (4.11), (4.15), and (4.16) using the central differencing approximation, we obtain four coupled tridiagonal equations. This system is solved iteratively by a conventional tridiagonal equation solver. Since the boundary conditions involve the derivatives of temperature and concentrations, difficulties arise in the numerical computations. Two key factors that influence the success of a stable computation are, first, the selection of the approximate forms of the initial profiles of temperature and concentrations, and, second, the correct iteration orders for these four governing equations.

The Appendix includes the computer code used here for the finite chemistry calculation. This particular computational procedure, running under double precision on IBM 3090-600s, works very well in representing the diffusion flame. Although it remains difficult to estimate its computational efficiency in the absence of standard-

ized initial conditions, the stability of the present computational method is found to be excellent. The domain of computation is selected to be from η=0 (liquid-gas interface) to η=20 (gas free stream) and 40 spatial grid points per unit length are used to perform sufficiently accurate calculations.

Typical results and corresponding phyiscal phenomena will be discussed in the following section.

4.3 Results and discussion

Illustrative calculations have been carried out for n-decane as a typical liquid fuel. The following physical properties can be used in a simple calculation:

$$\alpha = 15.5,$$

$$A_r = 1\times10^8,$$

$$E_a = 20 - 40 \ \ kcal/mole,$$

$$Le = Sc = Pr = 1,$$

$$T_w = 400\,K,$$

$$T_\infty = 1000\,K,$$

$$Y_{oe} = 1.0,$$

$$C_p = 1062 \ \ J/kg\ K,$$

$$Q = 2380.935 \ \ kJ/kg,$$

$Q_l = 321.079\ kJ/kg.$

The liquid temperature is assumed constant throughout the jet, as earlier studies have shown that for these types of liquid transverse jets, the heating of the liquid is negligible (see Nguyen (1989)).

Figures 16ab show the typical temperature distributions and mass fraction distributions at the stagnation point for incompressible and low subsonic cross flow. The peak in the temperature distribution together with the overlap of fuel and oxidizer in the reaction zone are indications of the flame location. The flame temperature increases to roughly twelve times the liquid surface temperature, after which the gas temperature drops to the free stream temperature asymptotically. The reaction zone thickness is finite here, under the finite rate chemistry assumption, but is still very thin, consistent with the relatively small activation energy used here. Especially for incompressible cross flow (M=0), the reaction zone thickness tends to go to the fast reaction rate limit, which means that with increasing compressibility the finite chemistry effects will be more significant. The solutions from Saitoh and Nagano (1979) for transient combustion of a fuel droplet with finite rate chemistry (see Figure 17) also have similar temperature and mass fraction distributions. In the present solution, by reducing the activation energy further, we can predict the flame and concentration characteristics in the limit of a fast reaction rate (Figure 18). We can also carry out the solutions for nearly frozen flow, the opposite extreme, by increasing the activation energy so that the chemical reaction proceeds at a negligible rate. Figure 19 is a typical solution for frozen flow.

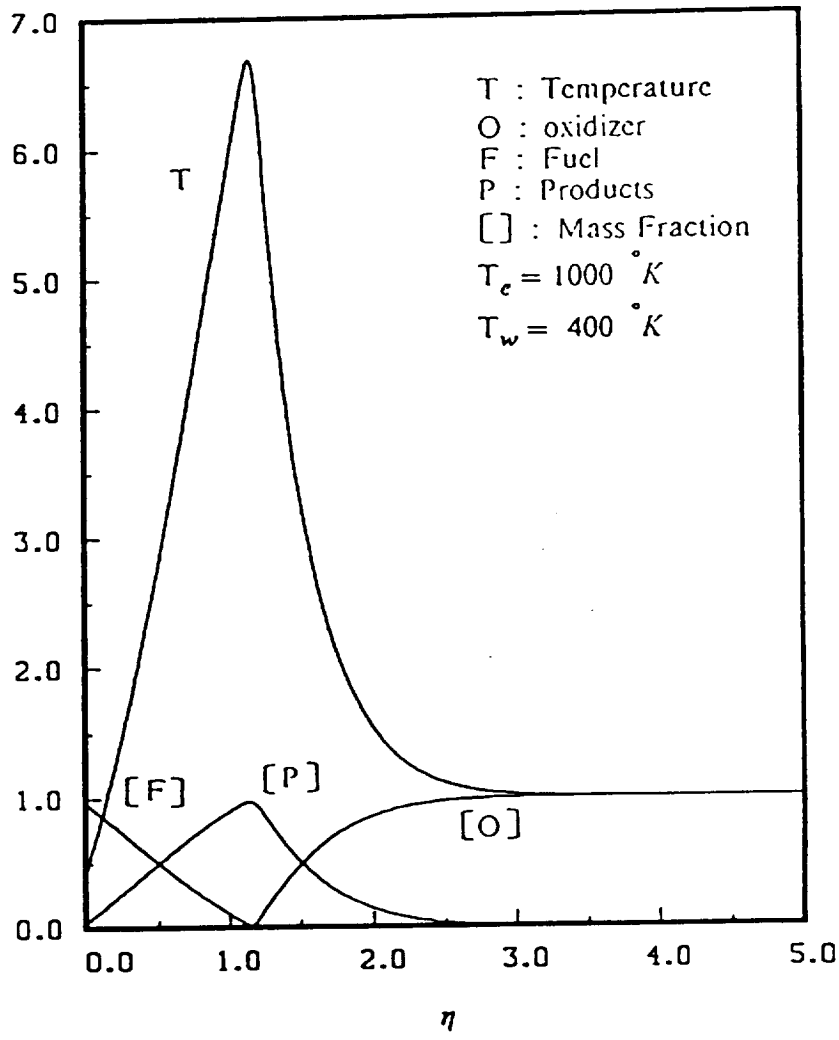

Figure 16a Typical flame structure at stagnation point for M=0.

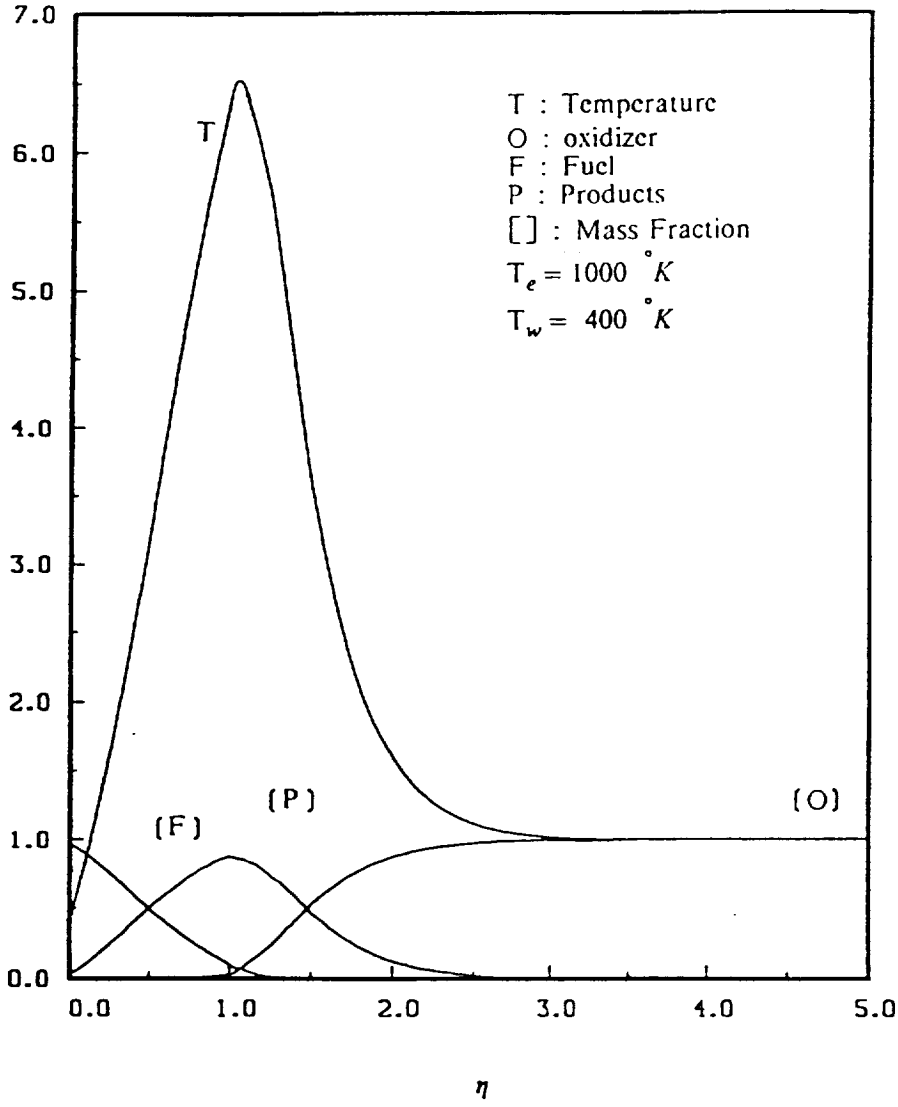

Figure 16b Typical flame structure at stagnation point for M=0.3.

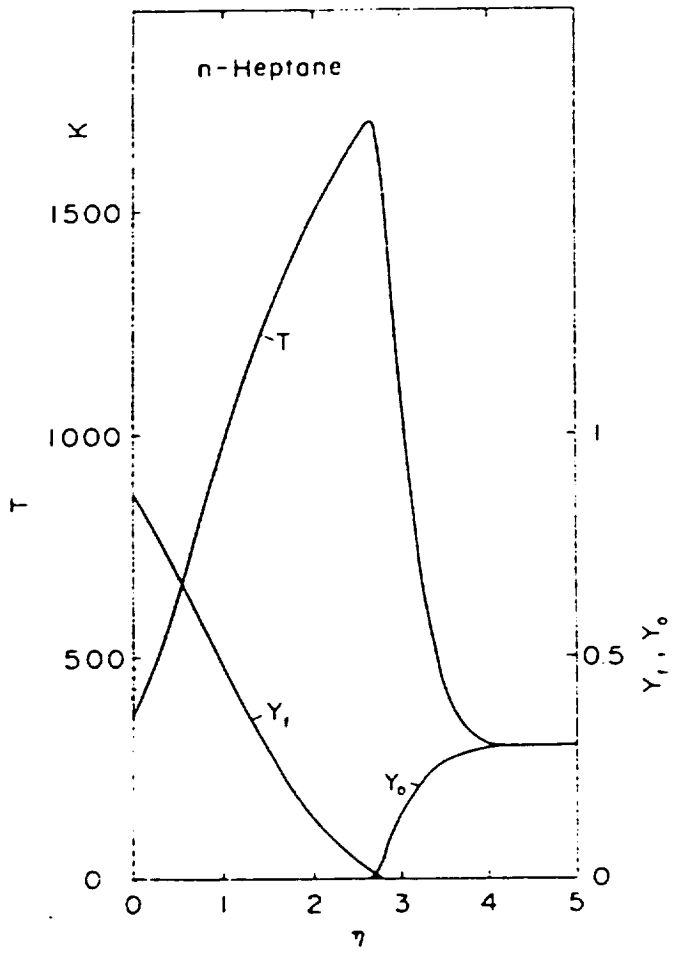

Figure 17 Typical flame structure from Saitoh and Nagano (1979).

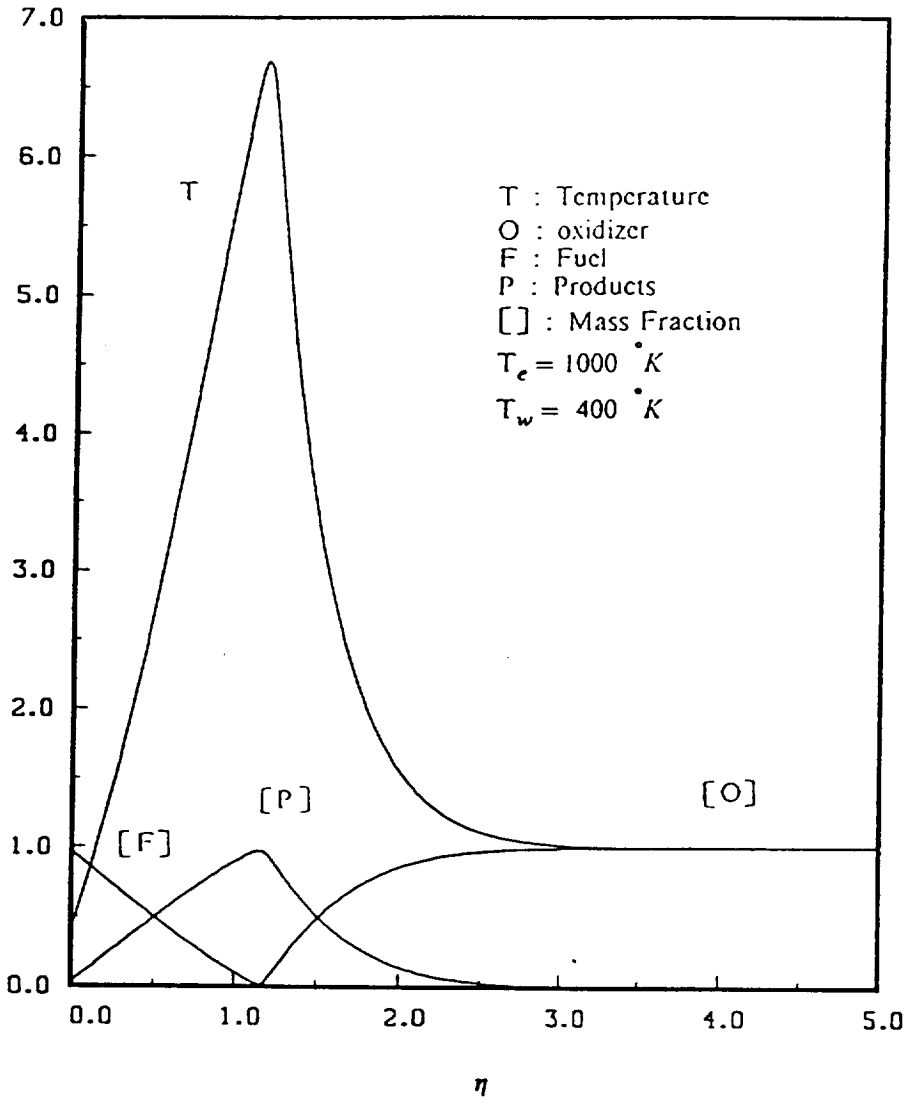

Figure 18 Flame structure for fast chemistry approximation at stagnation point for M=0.3.

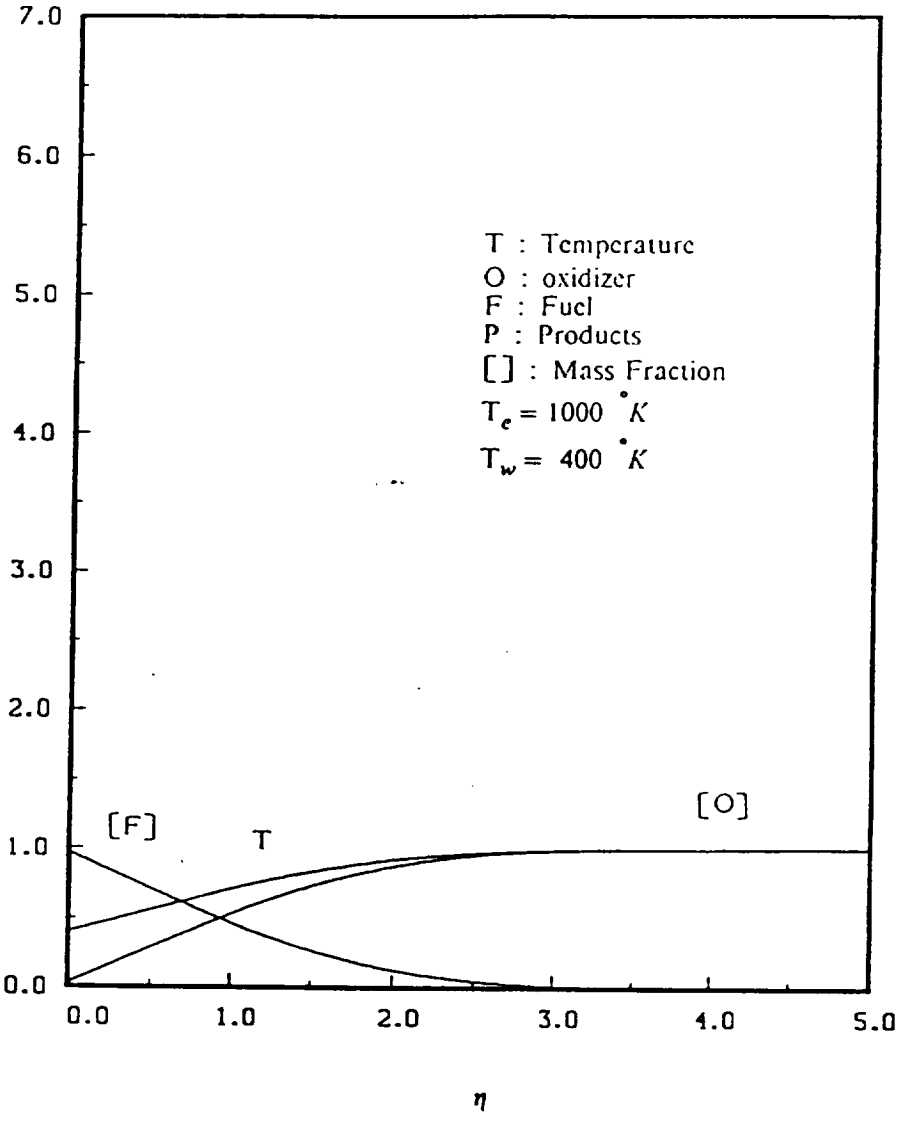

Figure 19 Flame structure for nearly frozen flow at stagnation for M=0.3.

Generally, in all these cases, the thermal boundary layers are confined within $\eta = 3.5$ and the flame location is at about $\eta = 1$ at the stagnation point of the ellipse. The information concerning the reactions occuring in the boundary layer can be used to study the overall combustion characteristics of the liquid fuel jet.

Figures 20-23 describe trends for the variation in the temperature and species concentrations corresponding to different locations along the elliptical surface, for different effective Mach numbers. As we move along the ellipse from the stagnation point, the flame appears to move away from the liquid surface, consistent with intuition and with the modeling of Nguyen (1989). At the same time, the mass fractions of fuel and oxidizer within the reaction zone are becoming smaller. Clearly, the convective effects,including ultimate separation of the boundary layer, cause the flame to move away from the surface, further from the supply of fuel vapor. Temperature distributions at various locations along the ellipse are shown in Figure 24 and 25. The maximum temperature tends to drop as one moves away from the stagnation point, consistent with the drop in the stagnation temperature of the gas near the surface away from the stagnation point.

Our main objective here is to identify the ignition position along the jet cross-section using the observations of previous researchers. Two alternative mechanisms were postulated by Kashiwagi and Summerfield (1972) as responsible for the development of ignition: (1) an exothermic gas-phase reaction in the boundary layer, and (2) a heterogeneous reaction at the interface. Each of the two theories takes into account the changing profiles within the boundary layer during the induction period prior to ignition, the simultaneously changing thermal profile below the

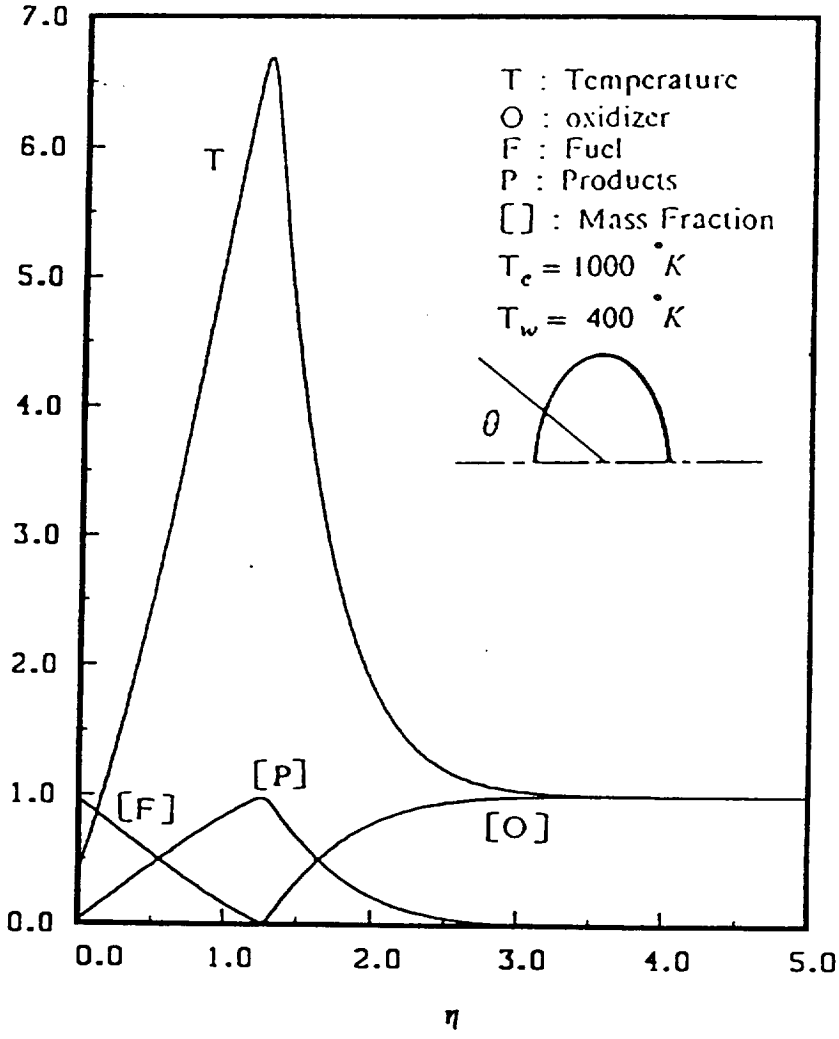

Figure 20 Flame structure for M=0 at ellipse surface θ =45°.

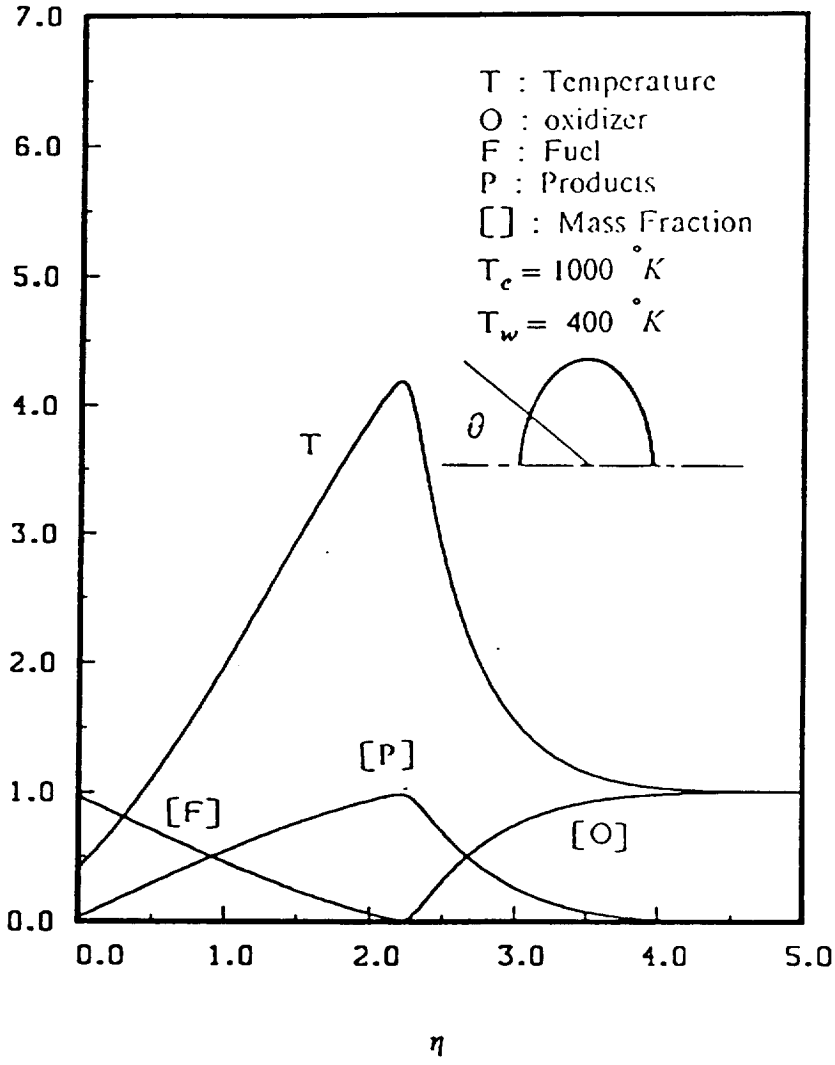

Figure 21 Flame structure for $M=0$ at ellipse surface $\theta = 90^o$.

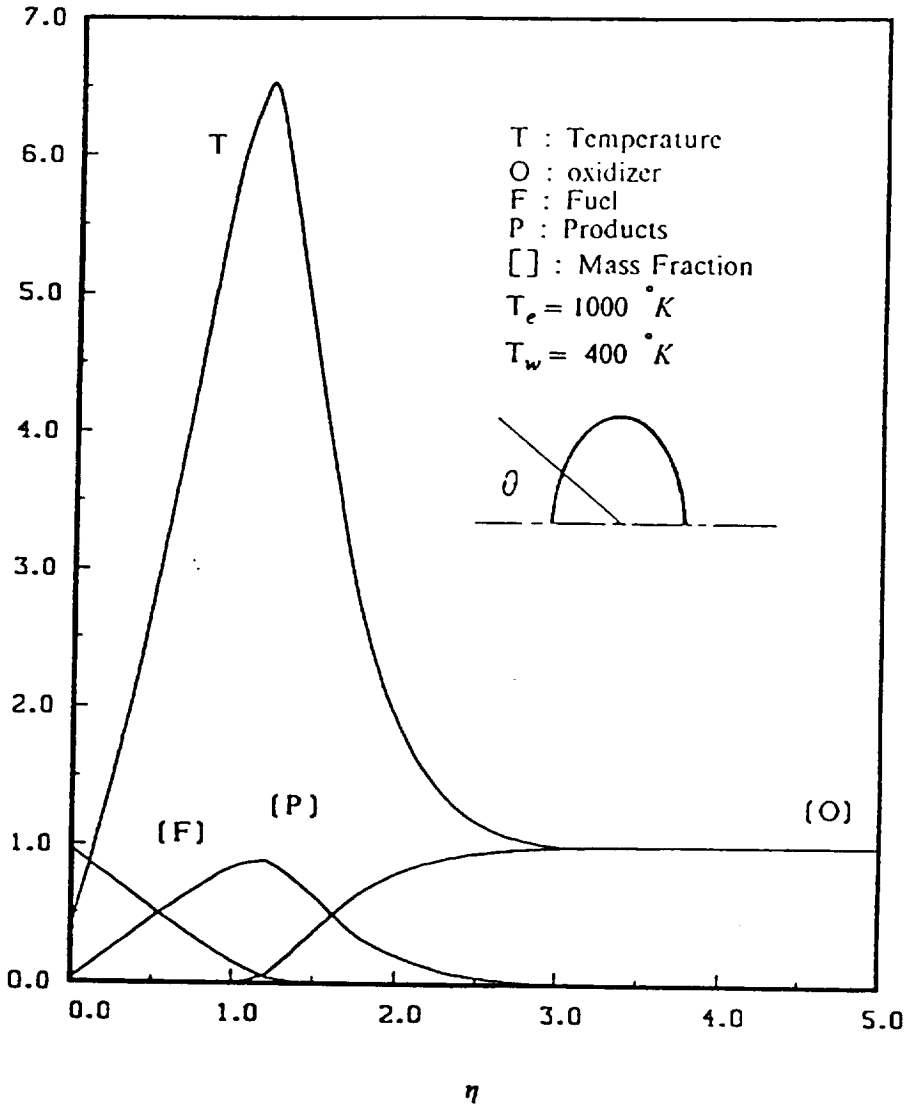

Figure 22 Flame structure for M=0.3 at ellipse surface θ =45°.

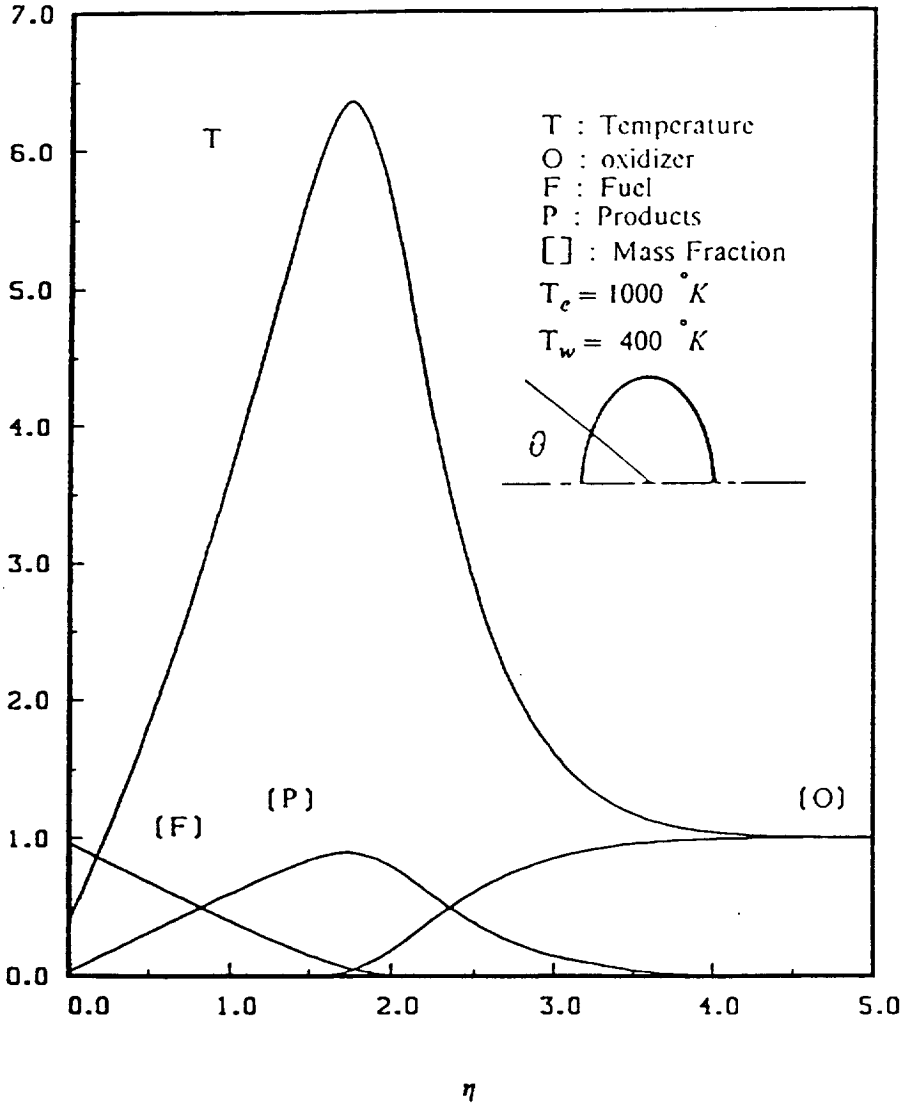

Figure 23 Flame structure for M =0.3 at ellipse surface θ =90°.

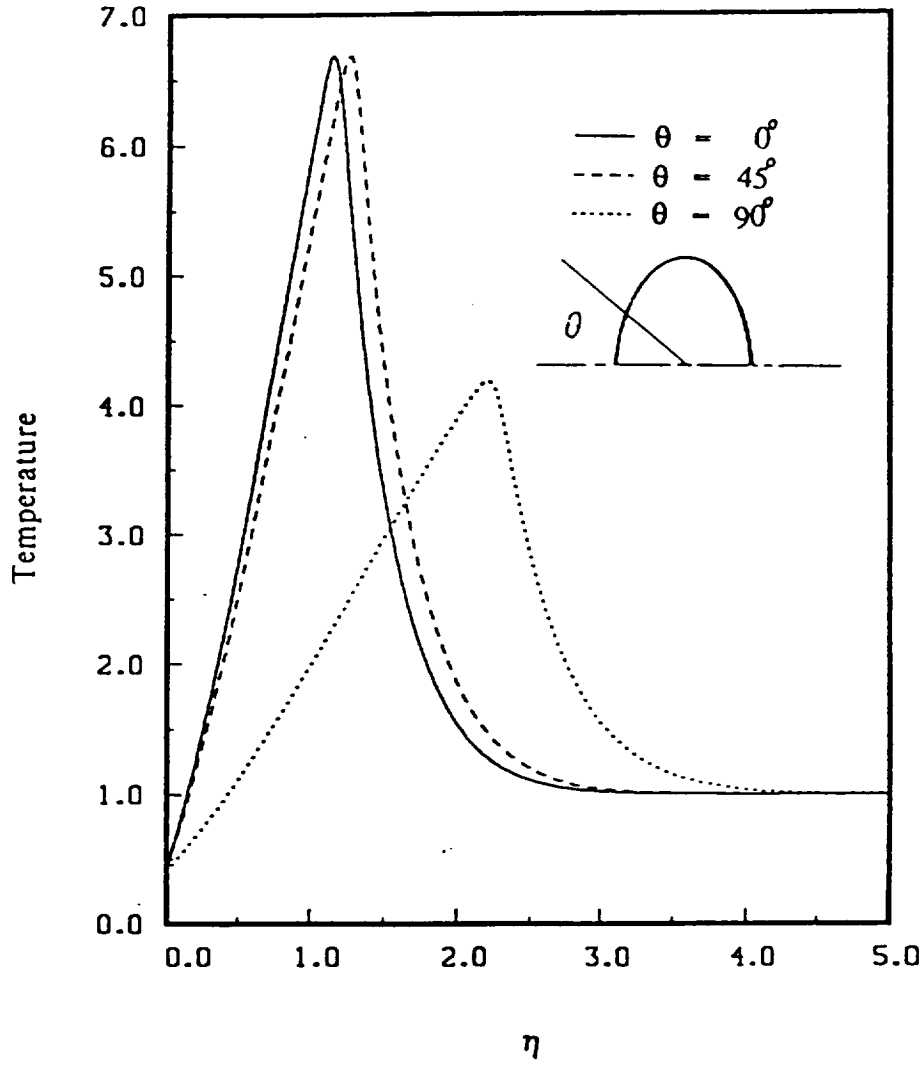

Figure 24 The variation of the boundary layer temperature distribution with location for $M=0$.

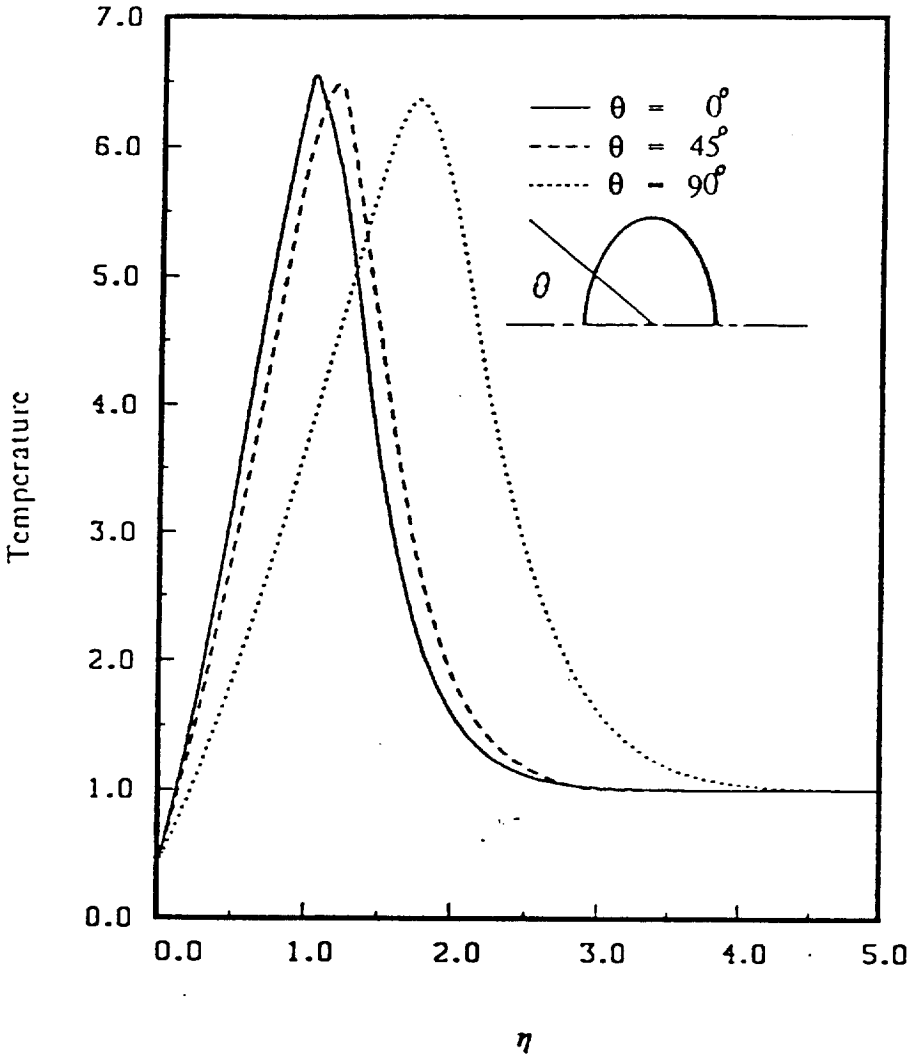

Figure 25 The variation of the boundary layer temperature distribution with location for M=0.3.

surface of the fuel due to convective heating, and the gradually rising rate of reaction. Ignition is said to occur at that time and that location at which the reaction rate reaches a suitablly defined "runaway" condition, or local maximum. In their theoretical studies, Kashiwagi and Summerfield found that, in convective ignition, an exothermic gas-phase reaction controls ignition, rather than an exothermic surface reaction. Therefore, an ignition criterion based on the gas-phase reaction rate is examined here, so that via the gas-phase model, the predicted ignition will occur at some downstream position along the jet cross-section, the distance increasing with increasing flow velocity and decreasing oxidizer concentration.

As shown in Figures 26a-d, the integrated values of reaction rate through the boundary layer are plotted as a function of non-dimensional distance along the cross-section boundary, $\bar{\xi} \equiv \frac{x}{h_0}$, where the h_0 is the half-spacing of the vortices. Note the change in scale between Figures 26ab and 26cd. The distribution of integrated reaction rate tends to have a maximum close to but not exactly coincident with the stagnation point, and falls off with $\bar{\xi}$ after $\bar{\xi}=10^{-1}$. This distribution, and its order of magnitude, are very similar to those observed by Kashiwagi and Summerfield (1972) (see Figure 27). As shown in Figures 26a-d, the global reaction rate increases with increasing effective Mach number, resulting from the higher stagnation pressure and higher maximum temperature in a flow with higher Mach number. The maximum in the integrated reaction rate also tends to move downstream of the stagnation point with increasing freestream Mach number. Using the local maximum in the integrated reaction rate, however, the predicted ignition position generally lies quite close to the stagnation point. While this result clearly indi-

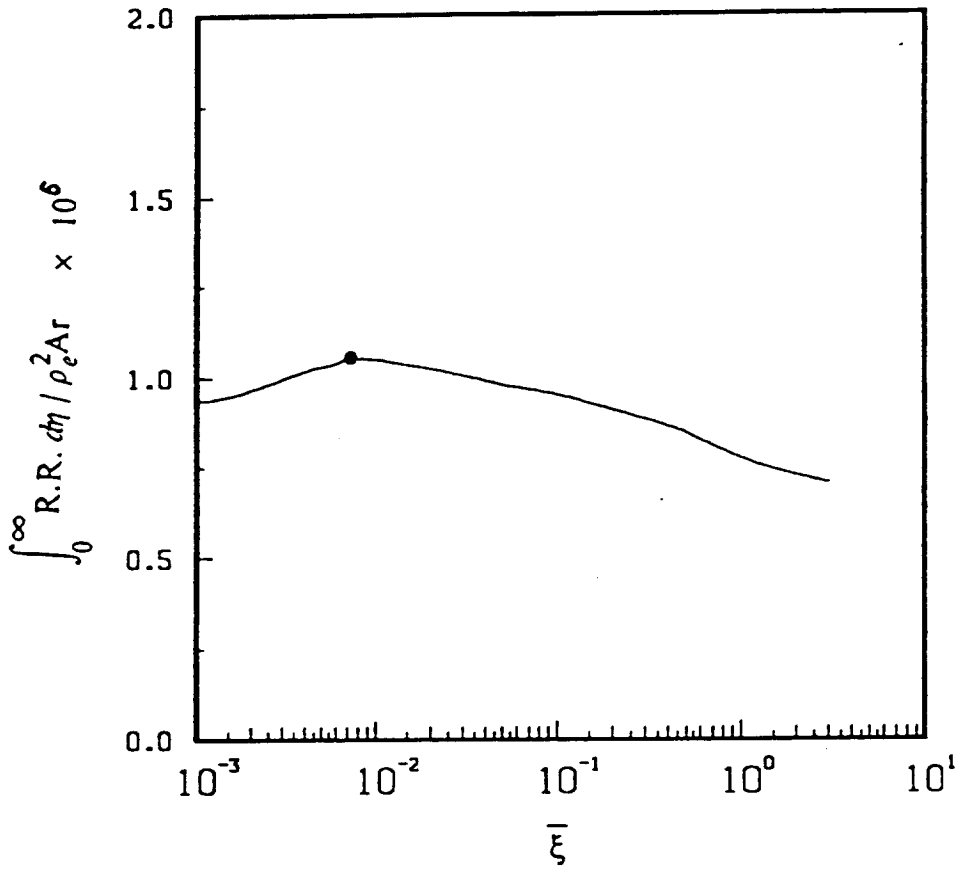

Figure 26a Distribution of integated reaction rate through boundary layer along ellipse surface ($\bar{\xi}$) for $M = 0$.

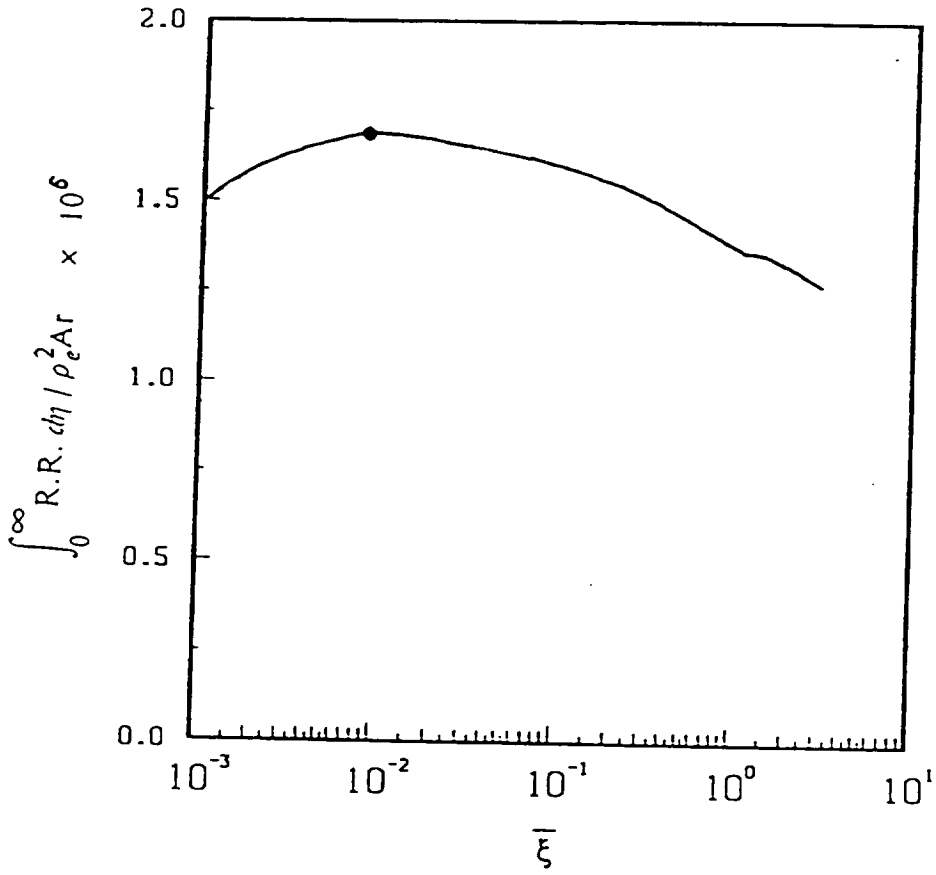

Figure 26b Distribution of integated reaction rate through boundary layer along ellipse surface ($\bar{\xi}$) for $M = 0.1$.

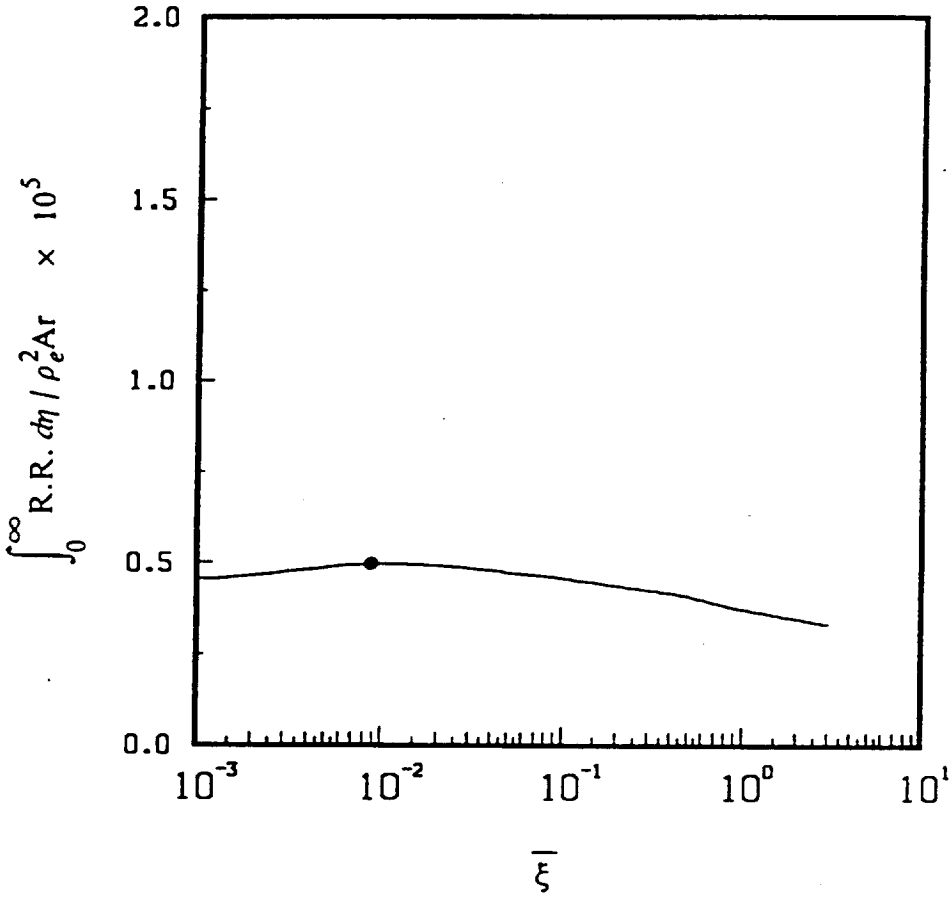

Figure 26c Distribution of integated reaction rate through boundary layer along ellipse surface ($\bar{\xi}$) for $M = 0.2$.

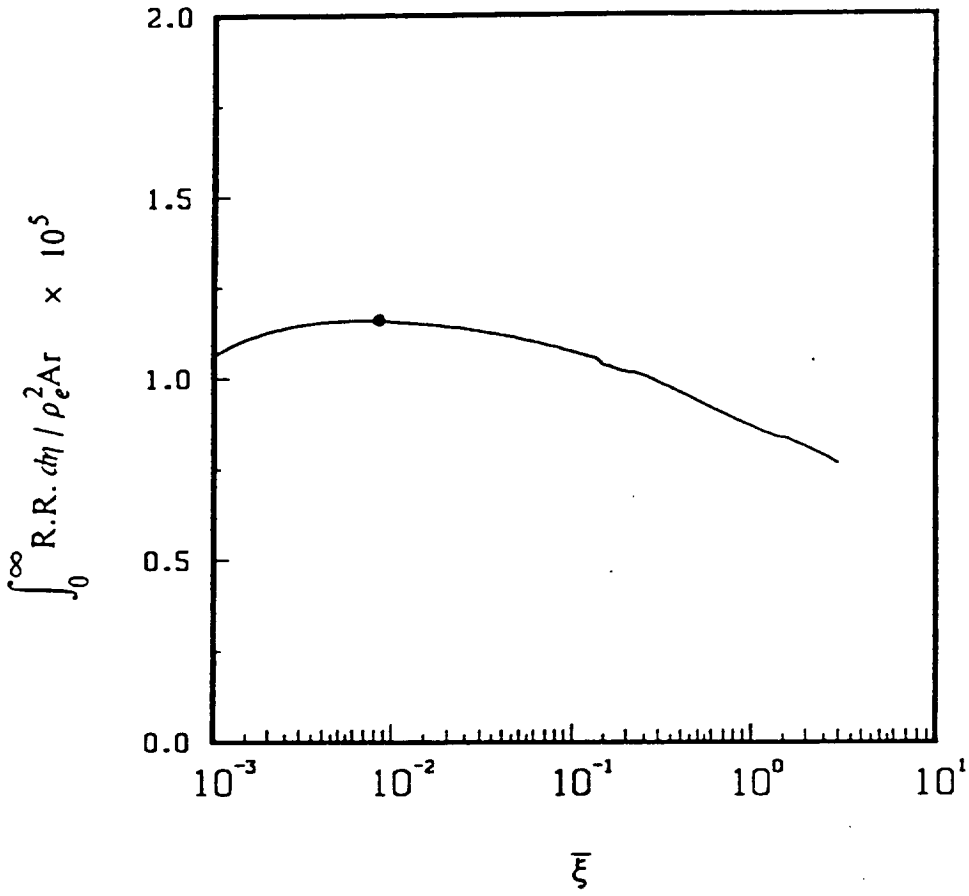

Figure 26d Distribution of integated reaction rate through boundary layer along ellipse surface ($\bar{\xi}$) for $M = 0.3$.

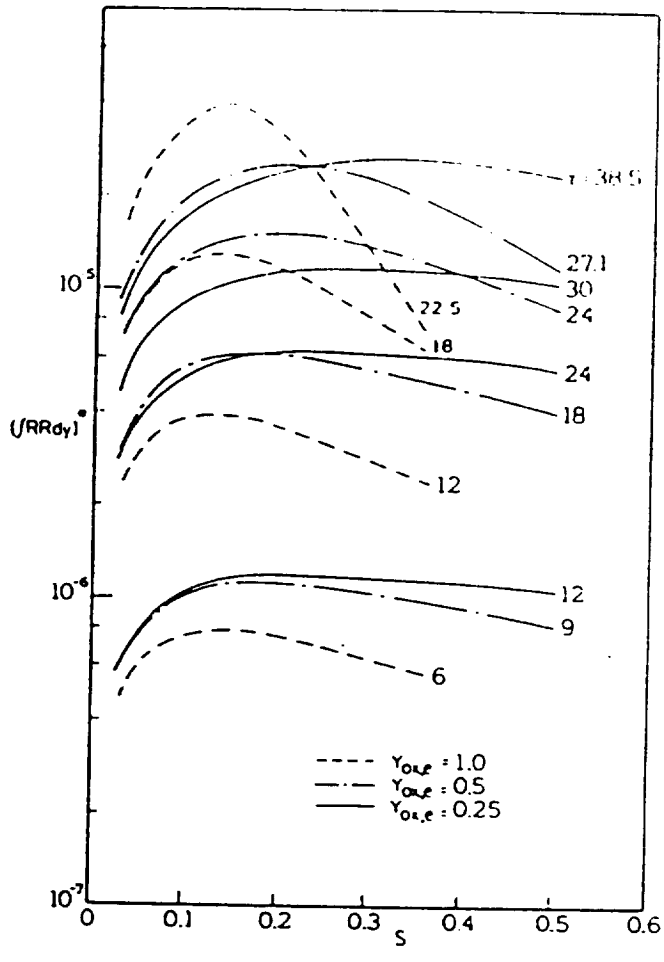

Figure 27 Distribution of integated reaction rate through boundary layer from Kashiwagi and Summerfield(1972) .

cates that ignition is likely under the low subsonic crossflow conditions, the observation that the ignition position moves downstream with increasing crossflow Mach number implies that ignition may be more difficult to achieve at higher Mach numbers.

The total mass of fuel consumed at a given location along the liquid jet by the flame can be found by integrating the reaction rate along the jet cross-section. This loss of mass by the jet results in a reduction in its local cross-sectional area. The plots in Figures 28-30 show the variation in effective jet cross-section area along the jet trajectory for different momentum flux ratios, upstream Mach numbers, and fuel types. At breakup locations on the order of 10 jet diameters downstream, the liquid jet cross-sectional area is still over 50 percent of its initial value. If the jet were to remain coherent downstream of 10 diameters, its area ratio would asymptote to a constant value by 20 diameters. Consistent with the reduced flame temperatures at lower freestream Mach numbers indicated in Figures 24-25, there is a smaller degree of mass loss by the jet at smaller values of M_∞ as indicated in Figures 28-30. The difference in jet axial velocity profile between present solution (see Figures 12a-e) and the constant velocity model used by Nguyen (1989) is believed to result in the difference in effective jet cross-section area in Figure 30. Finally, Figure 31 indicates the altered jet trajectory that can arise due to the mass loss computed and shown in Figures 28-30. As compared with the non-reacting jet trajectory, there is only a slight (5-10%) reduction in the degree of jet penetration when a reaction is present. The observations here are consistent with those of Nguyen (1989) and do not appear to be influenced strongly by the inclusion of finite rate chemistry.

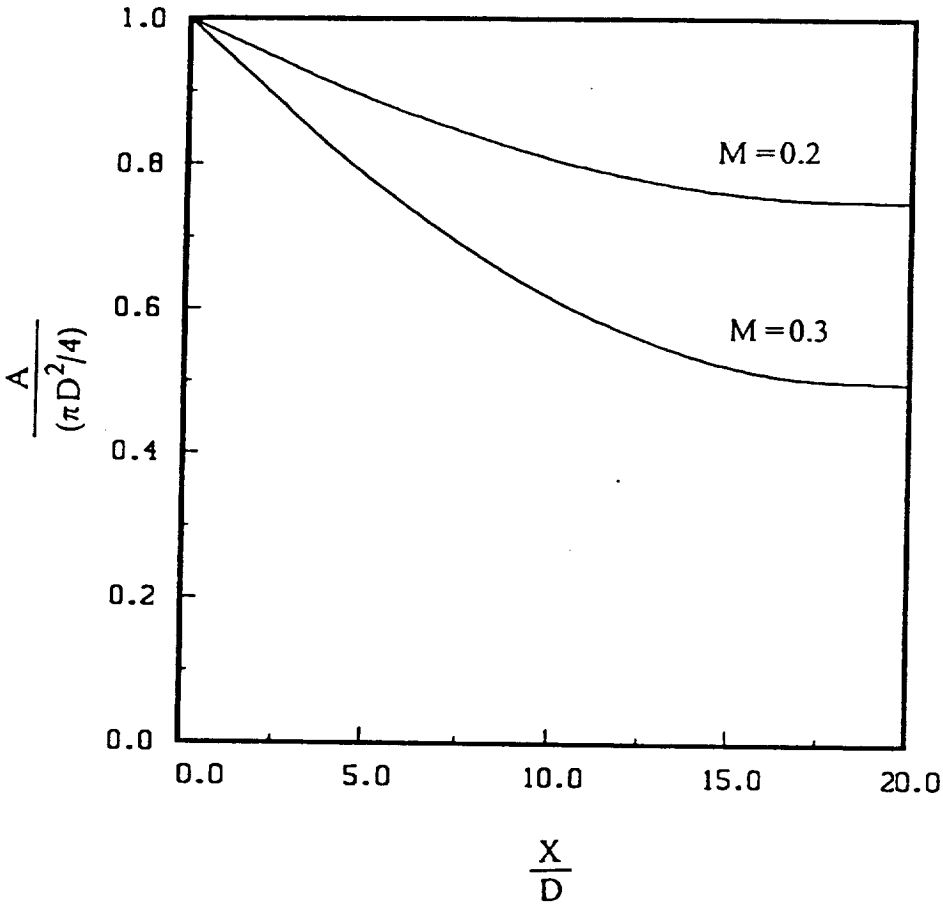

Figure 28 Effective jet cross-section area along the jet for $J=10$.

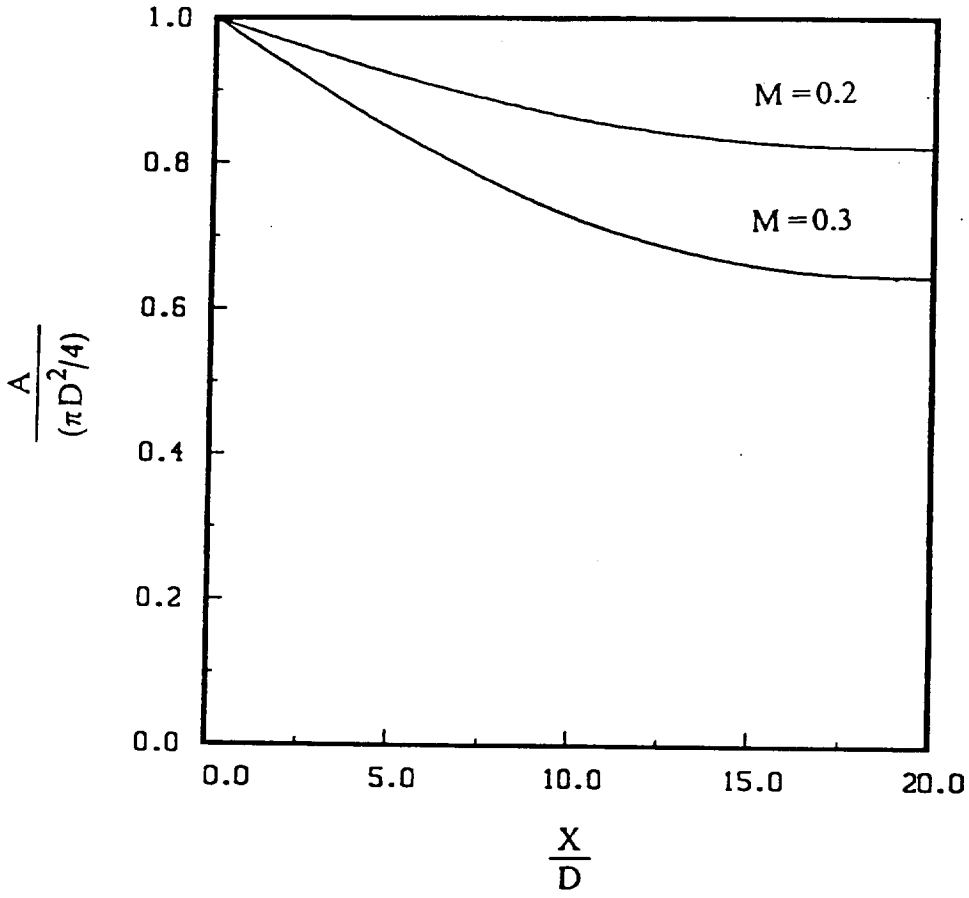

Figure 29 Effective jet cross-section area along the jet for J=20.

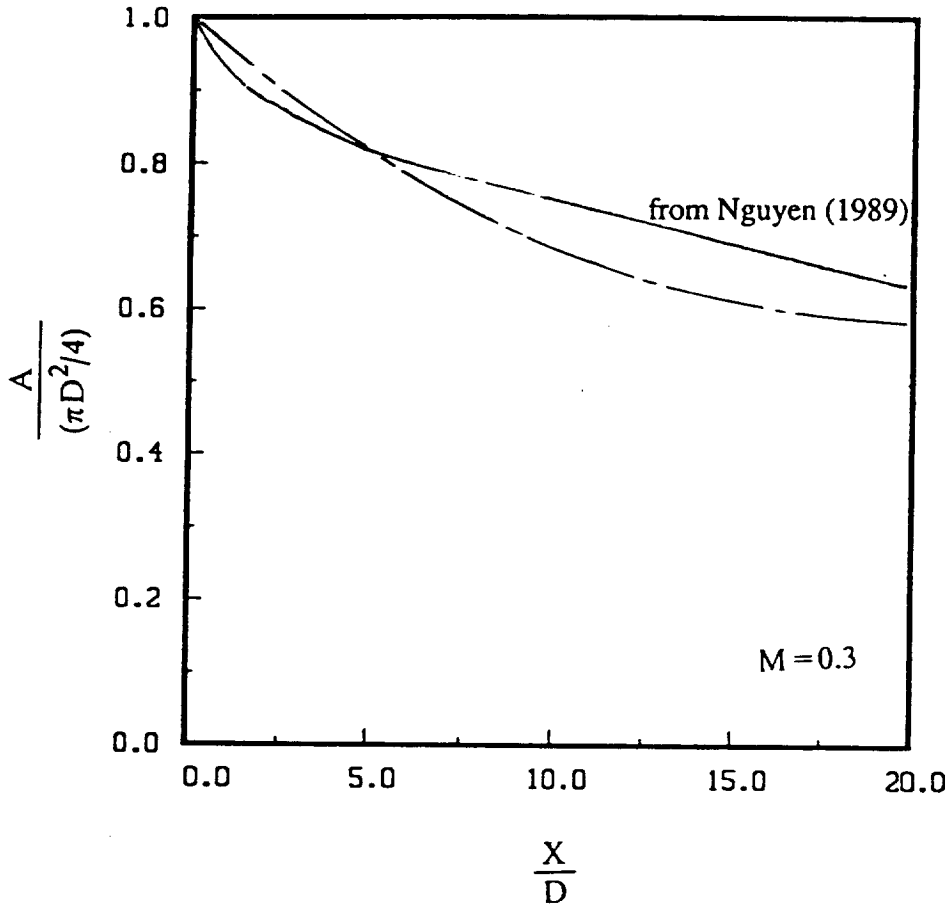

Figure 30 Effective jet cross-section area along the jet for $J=10$ and $B_o=2.5$ (compared with solution from Nguyen (1989)).

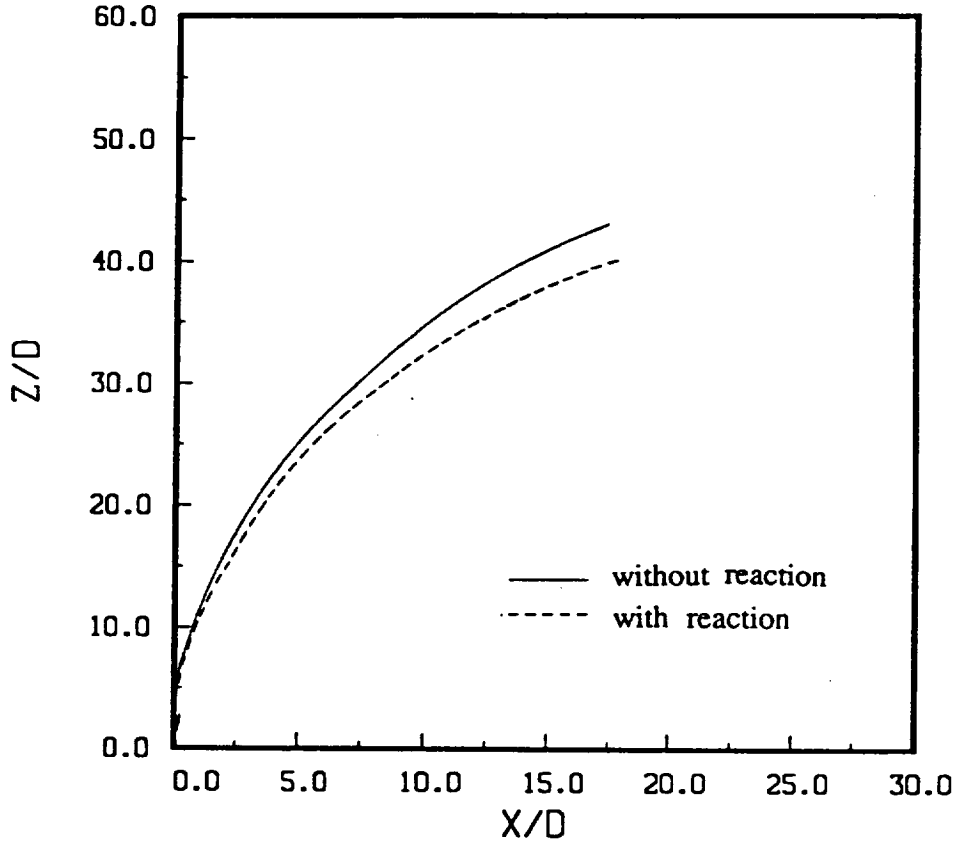

Figure 31 Computed jet trajectory for $M_\infty = 0.3, J = 10$.

CHAPTER V

CONCLUSIONS

In the present discussion of transverse liquid fuel jet breakup, burning, and ignition we have presented analyses which are rather general in nature such that they may also be useful in studying other types of transverse jet (e.g., gaseous) and non-equilibrium boundary layer problems. The results described in this thesis indicate that most of the features of the present analytical/numerical model accurately represent the flow phenomena associated with predicting liquid jet breakup in supersonic crossflow and burning in a low subsonic crossflow.

The current approach compares two different jet breakup criteria, the local sonic point vs. the "tension point" criterion, and indicates the sonic point criterion to be superior. Of course, inherent to the calculation of the local sonic point along the jet is the assumption that the actual jet trajectory after breakup is not significantly different from that which would occur without breakup. As indicated in Heister, et al. (1989), after 10 jet diameters, the experimentally observed trajectories do tend to lie 10-15% below the trajectories predicted using the assumption of a coherent liquid jet column. This difference in trajectory shape is not large enough to make a significant difference in the location of the sonic point. We might add that a reduced degree of penetration of the jet after breakup is consistent with the fact that the effective drag on the set of droplets comprising the jet cross-section is greater than the drag on the

single jet column.

While experimental data for nonequilibrium boundary layer and ignition positions for the transverse liquid fuel jet are not available, the numerical results for the nonequilibrium boundary layer by Chung (1965), for the fuel droplet with finite rate chemistry by Saitoh and Nagano (1980), and for hydrocarbon diffusion flame behavior by Jones and Lindstedt (1988) have been used to compare with the present flame structure solutions. The predicted temperature distributions, mass concentration distributions, and reaction rate distributions agree quite well with these previous solutions. The ignition position is found to be situated near the stagnation point of the jet cross-section, and it is observed that for higher free stream Mach numbers, the ignition position moves further downstream along the ellipse surface. To date, there are no papers available which describe experimentally the observed ignition position for the transverse liquid fuel jet. Future studies will concern the burning of transverse liquid fuel jets in higher upstream Mach number flows, incorporating numerical representation of the compressible gas phase flow.

REFERENCES

Adelberg, M. (1967) "Breakup Rate and Penetration of a Liquid Jet in a Gas Stream", **AIAA Journal, 5,** 1408-1415.

Baev, V. K., Shumskii, V. V., and Yaroslavtsev, M. I. (1983) "Self-Ignition of a Fuel Gas Escaping into an Oxidizing Medium", **Journal of Combustion, Explosive and Shock wave, 19,** 600-607.

Broadwell, J. E. and Breidenthal, R. E. (1984) "Structure and Mixing of a Transverse Jet in Incompressible Flow", **Journal of Fluid Mechanics, 148,** 405-412.

Brzustowski, T. A. (1976) "Flaring in the Energy Industry", **Progress in Energy and Combustion Science, 2,** 129-141.

Burke, S. P. and Schumann, T. E. W. (1928) "Diffusion Flames", **Ind. Eng. chem., 20,** 998.

Catton, I., Hill, D. E., and McRae, R. P. (1968) "Study of Liquid Jet Penetration in a Hypersonic Stream", **AIAA Journal, 6,** 2084-2089.

Chung, P. M. (1965) "Chemically Reacting Nonequilibrium Boundary layers", **Advances in Heat Transfer,** pp. 109-270, Academic Press, New York.

Clark, B. J. (1964) "Breakup of a Liquid Jet in a Transverse Flow of Gas", **NASA TN, D-2424.**

Crespo, A. and Linan, A. (1975) "Unsteady Effects in Droplet Evaporation and Combustion", **Combustion Science and Technology, 11,** 9-18.

Faeth, G. M. (1977) "Current Status of Droplet and Liquid Combustion", **Prog. Energy Combustion Science, 3,** 191-224.

Fearn, R. and Weston, R. P. (1974) "Vorticity Associated with a Jet in a Cross Flow", **AIAA Journal, 12,** 1666-1671.

Flugge-Lotz, I. and Johnson, A. F. (1955) "Laminar Compressible Boundary Layer along a Curved Insulated Surface", **Journal of the Aeronautical Sciences, 22,** 445-454.

Forde, J. M., Molder, S., and Szpiro, E. J. (1966) "Secondary Liquid Injection into a Supersonic Airstream", **Journal of Spacecraft and Rockets, 3,** 1172-1176.

Godunov, S. K., Zabrodin, A. V., and Prokopov, G. P. (1961) "A Computational Scheme for Two-Dimensional Non-Stationary Problems of Gas Dynamics and Calculation of the Flow from a Shock wave Approaching a Steady State", **U.S.S.R. Com-**

putational Mathematics and Math Physics, May, 1961.

Gonor, A. L. (1980) "Motion and Deformation of a Drop in a Gas Flow", **Fluid Mechanics - Soviet Researvch, 9,** 21-38.

Gruschwitz, E., **ONERA Publication,** No. 47, Paris, 1950.

Heister, S. D., Nguyen, T. T., and Karagozian, A. R. (1989) "Modeling of Liquid Jets Injected Transversely into a Supersonic Crossflow", **AIAA Journal, 27,** 1727-1734.

Heister, S. D. (1987) "Transverse Jets in Compressible Crossflows", **PhD Dissertation,** University of California, Los Angeles.

Jones, W. P. and Lindstedt, R. P. (1988) "Global Reaction Schemes for Hydrocarbon Combustion", **Combustion and Flame, 73,** 233-249.

Kamotani, Y. and Greber, I. (1972) "Experiments on a Turbulent Jet in a Cross Flow", **AIAA Journal, 10,** 1425-1429.

Karagozian, A. R. (1986a) "An Analytical Model for the Vorticity Associated with a Transverse Jet", **AIAA Journal, 24,** 429-436.

Karagozian, A. R. (1986b) "The Flame Structure and Vorticity Generated by a Chemically Reacting Transverse Jet", **AIAA Journal, 24,** 1502-1507.

Kashiwagi, T. and Summerfield, M. (1972) "Ignition and Flame Spreading over a Solid Fuel: Non-similar Theory for a Hot Oxidizing Boundary Layer", **Forteenth Symposium (international) on Combustion,** pp. 1235-1247.

Kolpin, M. A., Horn, K. P., and Reichenbach, R. E. (1969) "Further Experiments on Spreading of Liquids Injected into a Supersonic Flow", **AIAA Journal, 6,** 853-858.

Kou, K. K. (1986) **Principles of Combustion,** John Wiley & Sons, Inc.

Lees, L. (1956) "Laminar Heat Transfer over Blunt-nosed Body at Hypersonic Flight Speeds", **Jet Propulsion, 26,** 259.

Less, D. M., and Schetz, J. A. (1986) "Transient Behavior of Liquid Jet Injected Normal to a High-Velocity Gas Stream", **AIAA Journal, 24,** 1979-1986.

Nejad, A. and Schetz, J. A. (1972) "Effects of Viscosity and Surface Tension of Liquid Injectants on the Structure Characteristics of the Plume in Supersonic Airstream", **AIAA Paper,** 82-0253.

Nguyen, T. T. (1989) "Liquid Transverse Jets in Compressible Crossflow", **PhD Dissertation,** University of California, Los Angeles.

Nguyen, T. T. and Karagozian, A. R. (1989) "The Liquid Fuel Jet in Subsonic

Crossflow", AIAA Paper 90-0445, submitted to **Journal of Propulsion and Power.**

Saitoh, T. and Nagano, O. (1980) "Transient Combustion of a Fuel Droplet with Finite Rate of Chemical Reaction", **Combustion Science and Technology, 22,** 227-234.

Schetz, J. A., Kush, E. A., and Joshi, P. B. (1980) "Wave Phenomena in Liquid Jet Breakup in a Supersonic Crossflow", **AIAA Journal, 18,** 774-778.

Sherman, A. and Schetz, J. A. (1971) "Breakup of Liquid Sheets and Jets in a Supersonic Gas Stream", **AIAA Journal, 19,** 666-673.

Williams, F. A. (1985) **Combustion Theory** , The Benjamin/Cummings Publishing Compony, Inc.

APPENDIX

```
C
C
C   THIS PROGRAM IS TO SOLVE THE DIFFUSION FLAME WITHIN BOUNDARY
C   LAYER WITH FINITE RATE CHEMISTRY.
C
C
      IMPLICIT REAL*8(A-H,O-Z)
C
C     INITIALIZE THE FLOW PROPERTIES
C
      PARAMETER (H=0.025D0,N=401,ERR=1.D-7,TE=1000.D0,TW=400.D0,
     * PR=1.D0,SC=1.D0,AR=1.D8,VIS=41.9D-6,AEXP=10.071686D0,RO=1.765D0,
     * QF=4380.935D1,QO=683.03D0,QL=321.08D0,FM=142.29D0,CP=1.062D0,
     * U=186.06D0,URATIO=0.132D0,S=0.011D0,BETA=1.00D0,ALPHA=15.5D0)
      DIMENSION F(N),YO(N),YF(N),TEM(N),FF(N),FFF(N)
      COMMON/COM1/ C1(2000),D1(2000),E1(2000),B1(2000),NL
      UE=U*URATIO
      DAM=2.D0*AR*0.003D0*S/VIS/UE**2
      DQ=QF/(CP*TE*32.D0)
      DAT1=UE**2/(TE*CP*1000.0)
      B0=(CP*(TE-TW)+ALPHA*1.D0*QO)/QL
C
C     SET UP INITIAL GUESSES FOR MASS FRACTIONS AND TEMPERATURE
C
      NL=N
      N1=N-1
      F(1)=0.D0
      F(N)=1.D0
      TEM(1)=TW/TE
      TEM(N)=1.D0
      YO(1)=0.D0
      YO(N)=1.0D0
      YF(1)=B0/(1.D0+B0)
      YF(N)=0.D0
      DO 2 I=2,N1
      F(I)=(F(N)-F(1))/400.D0*(I-1)+F(1)
      TEM(I)=(TEM(N)-TEM(1))/400.D0*(I-1)+TEM(1)
      YO(I)=(YO(N)-YO(1))/400.D0*(I-1)+YO(1)
      YF(I)=(YF(N)-YF(1))/400.D0*(I-1)+YF(1)
    2 CONTINUE
      FF(1)=0.0D0
      DO 4 I=2,N
      FF(I)=FF(I-1)+H*F(I-1)
    4 CONTINUE
C
```

```
C    SOLVE EQUATION SYSTEM ITERATIVELY UNTIL THE LARGEST ERROR
C    IS LESS THAN 1E-7
C
     DO 100 M=1,500
     EMAX=0.0D0
C
C    MOMENTUM EQUATION
C
     DO 10 I=2,N1
     C1(I)=1.D0-FF(I)*H/2.D0
     D1(I)=-(2.D0+2.D0*H**2*BETA*F(I))
     E1(I+1)=1.D0+FF(I)*H/2.D0
     B1(I)=-BETA*H**2*(TEM(I)+F(I)**2)
  10 CONTINUE
     D1(1)=1.D0
     E1(2)=0.D0
     C1(N)=0.D0
     D1(N)=1.D0
     B1(1)=F(1)
     B1(N)=F(N)
     CALL TRI
     DO 12 I=1,N
     DTEMP=ABS(B1(I)-F(I))
     IF (EMAX.GT.DTEMP) GO TO 11
     EMAX=DTEMP
  11 F(I)=B1(I)
  12 CONTINUE
     IF (ERR.GT.EMAX) GO TO 101
     DO 9  I=2,N
     FF(I)=FF(I-1)+H*F(I-1)
   9 CONTINUE
C
C    SPECIES EQUATION FOR OXIDIZER MASS FRACTION
C
     DO 20 I=2,N1
     C1(I)=1.D0/SC-FF(I)*H/2.D0
     D1(I)=-2.D0/SC
    *    -H**2*DAM*ALPHA*YF(I)*EXP(-AEXP/TEM(I))/TEM(I)/FM
     E1(I+1)=1.D0/SC+FF(I)*H/2.D0
     B1(I)=0.0D0
  20 CONTINUE
     D1(1)=1.D0
     E1(2)=0.D0
     D1(N)=1.D0
     C1(N)=0.D0
     B1(1)=0.D0
     B1(N)=1.0D0
     CALL TRI
```

```
      DO 21 I=1,N
      YO(I)=B1(I)
   21 CONTINUE
C
C     SPECIES EQUATION FOR FUEL MASS FRACTION
C
      DO 22 I=2,N1
      C1(I)=1.D0/SC-FF(I)*H/2.D0
      D1(I)=-2.D0/SC
     *     -H**2*DAM*YO(I)*EXP(-AEXP/TEM(I))/32.D0/TEM(I)
      E1(I+1)=1.D0/SC+FF(I)*H/2.D0
      B1(I)=0.0D0
   22 CONTINUE
      D1(1)=1.0D0
      E1(2)=0.D0
      C1(N)=0.D0
      D1(N)=1.D0
      B1(1)=YF(1)
      B1(N)=YF(N)
      CALL TRI
      DO 24 I=1,N
      YF(I)=B1(I)
   24 CONTINUE
      DO 15 I=2,N1
      FFF(I)=(F(I+1)-F(I-1))/H/2.D0
   15 CONTINUE
C
C     ENERGY EQUATION
C
      DO 14 I=2,N1
      C1(I)=1.D0/PR-FF(I)*H/2.D0-(YO(I+1)-YO(I-1)+YF(I+1)-YF(I-1))/4.D0
      D1(I)=-2.D0/PR-H**2*DAT1*BETA*F(I)
      E1(I+1)=1.D0/PR+FF(I)*H/2.D0
     *       +(YO(I+1)-YO(I-1)+YF(I+1)-YF(I-1))/4.D0
      B1(I)=-H**2*DAM*DQ*YO(I)*YF(I)*EXP(-AEXP/TEM(I))/TEM(I)
     *       -H**2*DAT1*FFF(I)**2
   14 CONTINUE
      D1(1)=1.D0
      E1(2)=0.D0
      C1(N)=0.D0
      D1(N)=1.D0
      B1(1)=TEM(1)
      B1(N)=TEM(N)
      CALL TRI
      DO 18 J=1,N
      TEM(J)=B1(J)
   18 CONTINUE
      WRITE (6,199) M,EMAX
```

```
199 FORMAT(//,' ITERATION TIMES = ',I4,'   ERROR = ',D15.8)
100 CONTINUE
101 WRITE(6,200) M,EMAX
200 FORMAT(//,' ITERATION TIMES = ',I4,'   ERROE = ',D15.8)
    DO 112 I=1,N
    X=(I-1)*H
    PRO=1.D0-YO(I)-YF(I)
    WRITE(6,202) X,TEM(I),YO(I),YF(I),PRO
202 FORMAT(1X,F5.3,1X,4(D13.6,1X))
114 CONTINUE
112 CONTINUE
    WW=0.D0
    DO 212 I=2,N1
    WW=WW+2.D0*YO(I)*YF(I)*EXP(-AEXP/TEM(I))/TEM(I)**2
212 CONTINUE
    WW=WW*H/2.D0
    WRITE(6,222) WW
222 FORMAT(//,' R. R. = ',D15.8)
    STOP
    END
C
C
C    SUBROUTINE TRI IS TO SOLVE TRIDIAGONAL MATRIX UP TO 2000x2000
C
C
    SUBROUTINE TRI
    IMPLICIT REAL*8(A-H,O-Z)
    COMMON/COM1/ C1(2000),D1(2000),E1(2000),B1(2000),NL
    DO 10 I=2,NL
    E1(I)=E1(I)/D1(I-1)
    D1(I)=D1(I)-C1(I)*E1(I)
 10 CONTINUE
    B1(1)=B1(1)/D1(1)
    DO 20 I=2,NL
    B1(I)=(B1(I)-B1(I-1)*C1(I))/D1(I)
 20 CONTINUE
    N2=NL-1
    DO 30 I=1,N2
    N1=NL-I
    B1(N1)=B1(N1)-B1(N1+1)*E1(N1+1)
 30 CONTINUE
    RETURN
    END
```